RI 8307

Bureau of Mines Report of Investigations/1978

Chemical Flame Inhibition Using Molecular Beam Mass Spectrometry

Reaction Rates and Mechanisms in a Methane Flame Inhibited With 1.1% CF_3Br

UNITED STATES DEPARTMENT OF THE INTERIOR

Report of Investigations 8307

Chemical Flame Inhibition Using Molecular Beam Mass Spectrometry

Reaction Rates and Mechanisms in a Methane Flame Inhibited With 1.1% CF_3Br

By Joan C. Biordi, Charles P. Lazzara, and John F. Papp

UNITED STATES DEPARTMENT OF THE INTERIOR
Cecil D. Andrus, Secretary

BUREAU OF MINES

This publication has been cataloged as follows:

Biordi, Joan C

Chemical flame inhibition using molecular beam mass spectrometry; reaction rates and mechanisms in a methane flame inhibited with 1.1% CF_3Br / by Joan C. Biordi, Charles P. Lazzara, and John F. Papp. [Washington] : U.S. Dept. of the Interior, Bureau of Mines, 1978.

43 p. : ill., diagrs. ; 27 cm. (Report of investigations - Bureau of Mines ; 8307)

Bibliography: p. 31-34.

1. Flame - Analysis. 2. Flame spectroscopy. 3. Mass spectrometry. I. Lazzara, Charles P., joint author. II. Papp, John F., joint author. III. United States. Bureau of Mines. IV. Title. V. Series: United States. Bureau of Mines. Report of investigations - Bureau of Mines ; 8307.

TN23.U7 no. 8307 622.06173
U.S. Dept. of the Int. Library

CONTENTS

ILLUSTRATIONS

ILLUSTRATIONS--Continued

TABLES

CHEMICAL FLAME INHIBITION USING MOLECULAR BEAM MASS SPECTROMETRY

Reaction Rates and Mechanisms in a Methane Flame Inhibited With 1.1% CF_3Br[1]

by

Joan C. Biordi,[2] Charles P. Lazzara,[3] and John F. Papp[4]

ABSTRACT

The Bureau of Mines used molecular beam-mass spectrometry to determine the microstructure of a 10.1% CH_4-21.2% O_2-67.6% Ar-1.1% CF_3Br inhibited flame and its uninhibited analog, both stabilized at 32 torr on a cooled flat-flame burner. Composition profiles of atomic, radical, and stable species and temperature profiles for both flames were obtained and compared. Kinetic analyses of the profiles yielded values for the rate coefficients of several elementary methane flame reactions and information on the reactions of formation and decay of the observed halocarbon species. CF_3Br is judged to decay by thermal decomposition as well as by abstraction reactions, and the fluorocarbon chemistry occurring in the inhibited flame is due primarily to CF_2 radical reactions. Rate coefficients and mechanisms for reactions of the inhibitor-related species are given.

INTRODUCTION

Chemical flame inhibitors are considered to act by interfering with the normal chemical reaction paths of flame propagation. This Bureau of Mines report is one of a series that documents an effort to provide the basic flame data required to understand the mechanisms by which flame inhibitors operate at the molecular level.

In the preceding papers (4, 7-8)[5] we have reported on the general character of the microstructure of low-pressure methane flames containing a small amount of CF_3Br and on the detailed kinetics and mechanisms for a flame

---

[1] This report is a combined and expanded version of two articles published in the Journal of Physical Chemistry (12-13).

[2] Research chemist, Bureau of Mines, Washington, D.C., formerly with Pittsburgh Mining and Safety Research Center, Bureau of Mines, Bruceton, Pa.

[3] Research chemist, Pittsburgh Mining and Safety Research Center, Bureau of Mines, Bruceton, Pa.

[4] Research physicist, Pittsburgh Mining and Safety Research Center, Bureau of Mines, Bruceton, Pa.

[5] Underlined numbers in parentheses refer to items in the list of references preceding the appendixes.

containing 0.3% CF_3Br in comparison with its uninhibited analog. It was clear from examination of these flames that the fluorine part of the inhibitor molecule reacts rapidly in the flame, but it was not possible to detect the CF_3 radical despite the ability to detect and measure other flame radicals with mole fractions of 10^{-4} to 10^{-5}. It was found that although the H atom concentration was reduced at low temperatures in the inhibited flame relative to the clean flame, some manifestations of inhibition observed for other chemical inhibitors, such as HBr (52), were only marginally evident. We therefore chose to examine the detailed microstructure of a flame containing significantly more CF_3Br to improve our chances of observing the CF_3 radical, to look for more pronounced effects of the inhibitor, and to obtain more data for clarifying mechanisms in this complex reaction system.

EXPERIMENTAL WORK

Two flames were examined at 0.042 atm: an uninhibited, slightly lean CH_4-O_2-Ar flame, and a flame of similar stoichiometry containing initially 1.1% CF_3Br. These quenched, flat flames differ from those studied previously in initial mass flow rate and, therefore, in burning velocity. A burning velocity of about 48 cm sec^{-1} for the clean flame was found to give satisfactorily stable (for quantitative microstructure determinations) inhibited flames when the CF_3Br was added.

The molecular beam sampling mass spectrometric detection system was the same as described previously, as were the techniques for radical detection and measurement (4, 7-8). Only departures from previously described procedures will be given here.

The formaldehyde profiles, determined at 30 amu, were corrected for $C^{18}O$. The expression used for the correction is $I_{30(H_2CO)} = I_{30} - (^{18}O/^{16}O)\, I_{28}$, where $(^{18}O/^{16}O)$ is the ratio of the natural isotopic abundance of ^{18}O to ^{16}O and I is the measured mass spectral intensity of mass 30 and mass 28 ($C^{16}O$) as indicated. This correction was not made in previously reported profiles for H_2CO (7-8). The effect of this correction to flames I and II, the clean and 0.3% CF_3Br flames, respectively, was to reduce the maximum X_{H_2CO} by 15% in flame I and 25% in flame II and to eliminate the apparent residual H_2CO in the secondary reaction zone.

The change in initial mass flow rate (burning velocity) for the clean flame from that previously used resulted in a different final flame temperature. The area expansion ratio profile was also different at the lower linear flow velocity. The characteristics of the two flames studied here, flame III and flame IV, as well as the two flames examined previously, flame I and flame II, are given in table 1. Flame temperature profiles were measured using fine wire platinum versus platinum-10% rhodium thermocouples coated with silica to minimize surface radical recombination. A temperature correction was made for the radiant energy loss of the thermocouple.

TABLE 1. - Characteristics of flames examined at 0.042 atm

	Flame I	Flame II	Flame III	Flame IV
Flow, g sec^{-1}:				
CH_4	0.0182	0.0182	0.0107	0.0108
O_2	0.0763	0.0765	0.0456	0.0455
Ar	0.3005	0.3002	0.1811	0.1808
CF_3Br	0	0.0047	0	0.0110
CH_4 mole-pct	10.3	10.3	10.1	10.1
O_2 mole-pct	21.6	21.6	21.5	21.2
Ar mole-pct	68.1	67.8	68.4	67.6
CF_3Br mole-pct	0	0.3	0	1.1
V_o [1] cm sec^{-1}	79.3	79.5	47.6	48.0
T_{max} [2] K	1,868	1,911	1,781	1,966
T_{ad} [3] K	2,379	2,374	2,375	2,358
A [4]	1.0+0.13z	1.0+0.13z	1.0+0.35z	1.0+0.35z

[1] Calculated using $T_{initial}$ = 298 K.
[2] As determined in the absence of the sampling probe (5).
[3] Calculated adiabatic flame temperature.
[4] Area expansion ratio (dimensionless) expressed as a function of distance from the burner surface, z, in centimeters, for $0<z<1$ cm.

Mass spectral sensitivities for CH_3Br, CH_2CF_2, F_2CO, HF, and Br in the 1.1% CF_3Br flame were determined by direct comparison with the flame containing initially 0.3% CF_3Br. That is, the 0.3% CF_3Br flame served as the calibration standard for the named species in the 1.1% CF_3Br flame. For CH_3Br (±10%), CH_2CF_2 (±2%), and F_2CO (±18%), the relative ionization cross-section calculations were also performed in the manner previously described (7) and the percent variation between the two approaches is given in the parentheses. This agreement gives an indication of the precision of the cross-section calculations from one set of ionizer conditions to another. For HBr (±8%), Br (<1%), and HF (±6%) conservation of mass calculations showed good agreement, as noted parenthetically, with the 0.3% CF_3Br flame calibration procedure, and this is an indication of the precision with which these flames can be reproduced on the burner over extended periods of time.

For CF_3Br, the initial points of the profile were set equal to the known, initial CF_3Br concentration. This is a more reliable procedure for CF_3Br than calibration with the initial, cold gas mixture because of possibly different temperature dependencies in the scattering function for CF_3Br and Ar, and the possible temperature effects on the CF_3Br fragmentation pattern. Both of these effects are quantitatively unknown, but since the temperature over the initial portion of the profile reaches 900 K, the procedure adopted essentially corrects for them up to that temperature.

In addition to the CF_2 radical (11), two other previously unobserved species, CF_3H and Br_2, were observed and measured. CF_3H was monitored as CHF_2^+ at mass 51, corrected for ^{13}C contributions from CF_2^+ at mass 50. The latter ion is formed from several other inhibited flame species. At the position in the flame for which CF_3H is a maximum, these corrections amounted to 10% of the observed intensity at 51 amu. An ionization efficiency curve for 51 amu

determined at the maximum yielded an appearance potential of 15.4±0.5 ev. The lowest reported appearance potential for CHF_2^+ from CF_3H is 15.75 ev (36). Other compounds (21) for which CHF_2^+ appearance potentials have been reported can be eliminated, either on the basis of their appearance potentials or because of lack of supporting mass spectral evidence for their existence in this flame. Lifshitz and Long (35) calculated a value of 15.7 ev for CHF_2^+ from CH_2CF_2, which is present in the flame, but consider that the rearrangement required to give this ion has a very low probability of occurrence. The profiles of mass 64 and mass 51, determined simultaneously in order to test this conclusion, are sufficiently different to insure that they derive from different species. The cross-section technique (11) was used to estimate the CF_3H concentration. Two calculations were made, one with the comparison ion CF_2^+ at 50 amu from CF_3Br, and one with FCO^+ at 47 amu from F_2CO. The results were the same to ±10%.

Br_2 was identified by its characteristic triplet at 158-160-162 amu, a feature not observed in the mass spectrum of CF_3Br or HBr. The uncertainty in the absolute concentration of Br_2 is large because of the need to estimate a partial ionization cross section for CF_3Br^+, the only possible comparison ion to minimize discrimination in the mass filter. The calculated value for $X_{Br_2}(max)$, $\sim 3\times10^{-5}$, is probably good only to within an order of magnitude.

The physical model and computational techniques used to analyze the profile data as well as a program listing and output for one flame have been published (40). From the concentration profiles, profiles of fractional mass flux, G_i, are calculated for each species according to the equation

$$G_i = \left[\frac{M_i}{\sum X_i M_i}\right]\left\{X_i - \left(\frac{D_{i-Ar}}{v}\right)\left[\frac{dX_i}{dz} + k_{T_i}\frac{d\ln T}{dz}\right]\right\}, \qquad (A)$$

where z is the perpendicular distance from the burner surface, X_i denotes mole fraction, M_i molecular weight, D_{i-Ar} the binary diffusion coefficient with argon, k_{T_i} the binary thermal diffusion ratio with argon, and v the average bulk flow velocity. Individual species net reaction rates, the sum of the rates of all reactions forming and all reactions consuming a given species, are calculated as

$$K_i = \frac{\rho_o v_o}{A M_i}\left(\frac{dG_i}{dz}\right), \qquad (B)$$

where ρ_o and v_o are the cold gas density and velocity, respectively, and A is the area expansion ratio. These net reaction rates, together with the concentrations and temperatures at each position in the flame, are the starting point from which kinetic analyses and deductions about mechanisms are made.

Application of the requirements of conservation of matter at the atomic level provides a test of the internal consistency and accuracy of the concentration profiles and their reduction to flux profiles (22). At each point in the flame the deviation of the net flux of any atomic species from its known inlet flux should be zero. Figure 1 shows the deviation in percent for C, H, and O in flames III and IV, and for F and Br in flame IV. Figure 1D is the

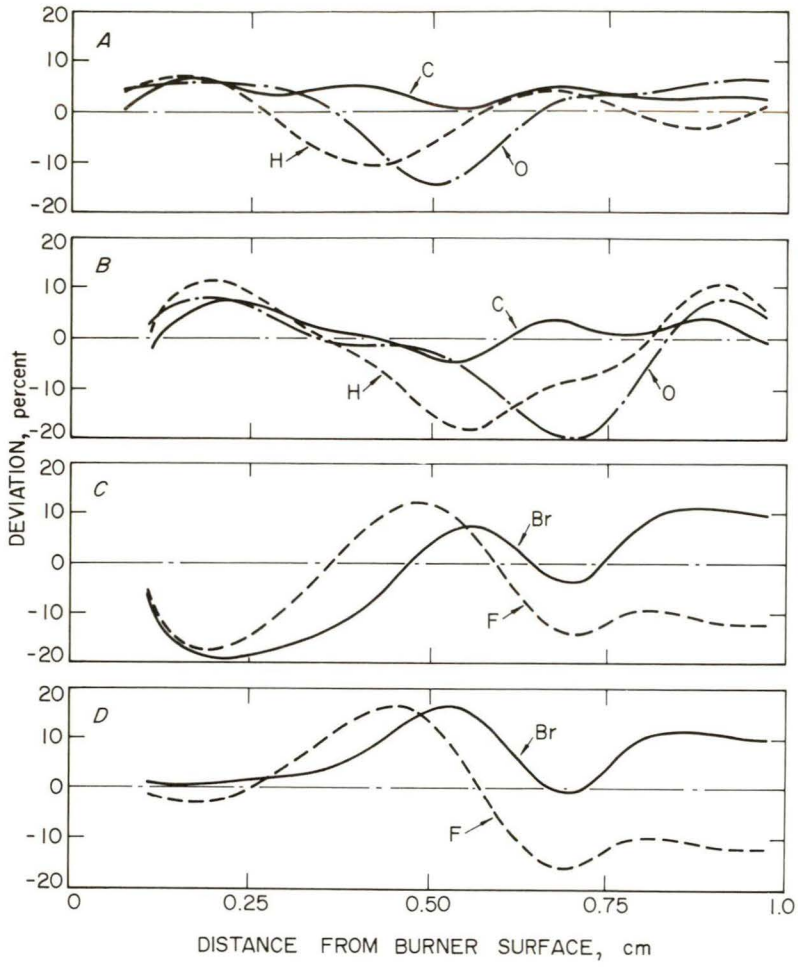

FIGURE 1. - Element conservation for clean and inhibited flames. *A*, Carbon, hydrogen, oxygen in flame III; *B*, carbon, hydrogen, oxygen in flame IV; *C*, bromine and fluorine in flame IV; *D*, same as in *C* except thermal diffusion is ignored.

result of a calculation for flame IV in which k_T was set equal to zero. This calculation suggests that part of the reason for the low F and Br flux at low values of z, where the CF_3Br profile is nearly flat, is an error in evaluation of the thermal diffusion flux for the inhibitor. Whether this is due primarily to the use of unrealistic molecular parameters (40) in calculating k_T for CF_3Br or in probe perturbation to the temperature gradient close to the burner surface is not known. In the region of the flame where the magnitude of the CF_3Br net reaction rate is near its maximum, T~1,650 K, and at higher temperatures, the thermal diffusion term makes a negligible difference in K_{CF_3Br}. Thus, calculations of reaction rate coefficients involving CF_3Br in this part of the flame are not strongly affected by the modeling of thermal diffusion. At lower temperature--for example, at 1,400 K where $|K_{CF_3Br}| \sim 0.1 |K_{CF_3Br}|_{max}$--the magnitude of the net reaction rate is about 50% higher with $k_T = 0$.

The broad, qualitative description of the complex experimental and analytical procedures used to gather the data of this report is admittedly written for readers familiar with the conventional technique of flame microstructure and with our previous communications on this subject. Further information on conventional techniques is available elsewhere (22). The details of our experiments have been published with respect to construction of the burner, probe, and detector and their performance (4), temperature measurements (4), the problem of probe perturbation to the flame (5), the identification and measurement of radical species in the flame (34), data reduction techniques (40), and applicability of these techniques to the determination of rate coefficients for reactions occurring in flames (7, 10).

RESULTS AND INTERPRETATION

Composition

As before, the complete microstructure of a clean flame and its inhibited analog were determined. Figures 2 and 3 show the mole fraction species profiles measured for the uninhibited flame III, $z \leq 1$ cm. Figures 4 through 7 show the mole fraction species profiles measured for the inhibited flame IV containing 1.1% CF_3Br. The temperature profiles determined for these flames are also shown and they have been shifted to account for the probe cooling effect described previously (5).

In these figures, the symbols are the data points and the lines through them are the results of applying smoothing techniques (40) to the data points for the purpose of calculating smooth first and second derivatives. Profiles were actually measured, though with a smaller density of data points, as far as z = 13 cm, with smoothing techniques applied using data points out to 1.7 cm. The ostensibly too low, flat portion of the Br curve reflects the average of all these data points. The H, O, and OH profiles shown here appear to be inconveniently truncated at z = 1 cm. Extended profiles of these species are given in reference 9. No attempt was made to measure the radicals HCO and HO_2 in either flame, although both had been observed in earlier studies. Appendix A contains a partial computer listing (every fifth point) of the smoothed mole fraction profiles for flames III and IV.

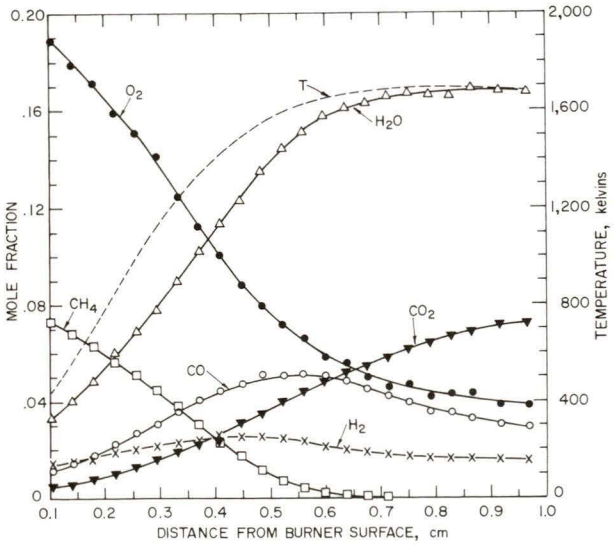

FIGURE 2. - Temperature and composition profiles for the major stable species of the uninhibited flame III.

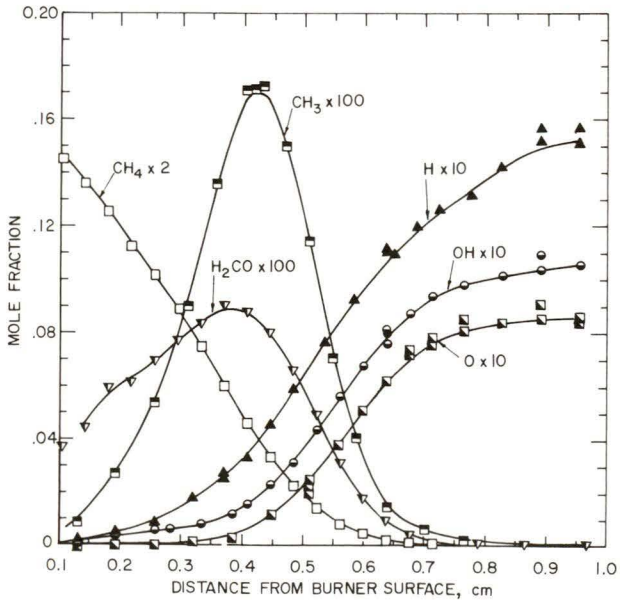

FIGURE 3. - Temperature and composition profiles for the major radical species and formaldehyde in the uninhibited flame III.

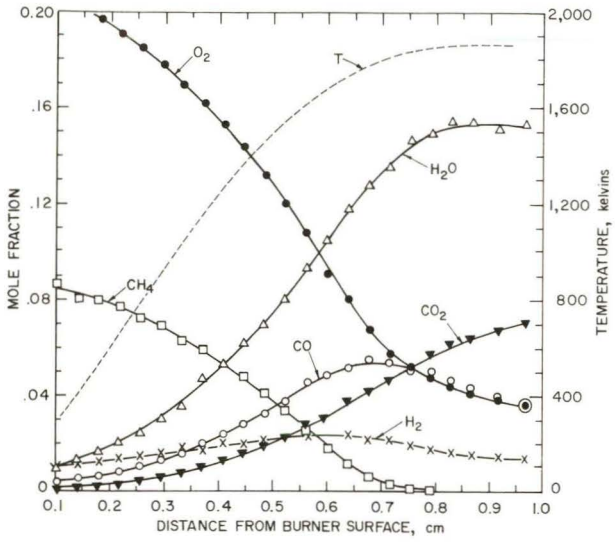

FIGURE 4. - Temperature and composition profiles for the major stable species unrelated to the inhibitor in flame IV.

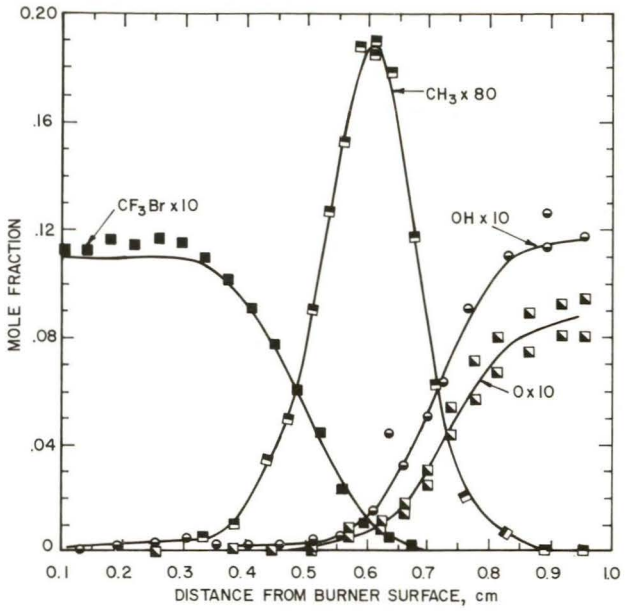

FIGURE 5. - Temperature and composition profiles of principal unstable species (except H) and the inhibitor, flame IV.

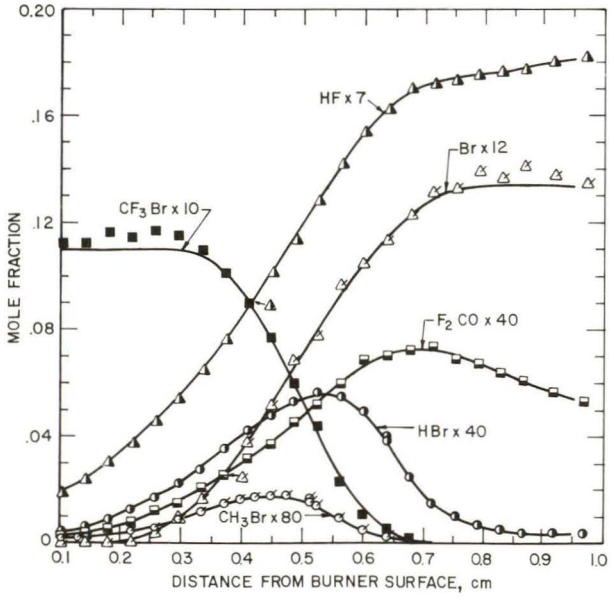

FIGURE 6. - Temperature and composition profiles for the major stable species related to the inhibitor in flame IV.

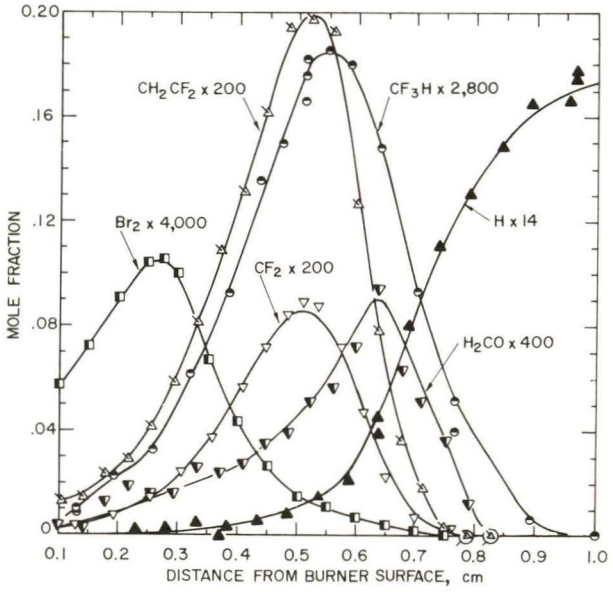

FIGURE 7. - Composition profiles for minor intermediate species, both stable and unstable, and for H atom, flame IV.

A comparison of the maximum concentrations of species related to the inhibitor in flames containing 0.3% and 1.1% CF_3Br initially shows them to be three to four times greater in the latter flame. This corresponds roughly to the ratio of initial CF_3Br concentrations and implies that there are no marked changes in the mechanism of formation and decay of these species between the two inhibited flames. In detail, of course, this must depend upon the relative temperature dependencies of the reactions involved. CF_3H and Br_2 have maximum mole fractions of 6.6×10^{-5} and 2.6×10^{-5}, respectively, in flame IV. They were not observed in the 0.3% CF_3Br flame, probably because one-third to one-fourth of these maxima is near the limit of detection for our apparatus as presently used. For the same reason, we could not unambiguously detect the CF_3 radical in either flame. However, the observation of CF_3H provides a route for calculating the concentration profile for CF_3 (11). This calculation gives a maximum mole fraction of CF_3 of about 3×10^{-5} occurring at $z = 0.52$ cm in flame IV. Because the appearance potential for CF_3^+ from CF_3 is only 2 ev less than that from CF_3Br, and because of the relatively broad electron energy spread of the ionizer, it is not surprising that such a small contribution to the 69-amu intensity could not be identified in the "tail" of the relatively very strong signal from CF_3Br.

Rate Coefficients of Elementary Flame Reactions

The net reaction rate profiles calculated according to equations A and B are shown in figures 8 and 9 for all the stable species not related to the inhibitor in flames III and IV, respectively. The net reaction rate for each species, K_i (moles cm^{-3} sec^{-1}), is plotted versus z(cm), the distance of the sampling probe from the burner surface. The bumps and shoulders exhibited by several of the rate profiles in figures 8 and 9 are due to small local variations in the smoothed mole fraction data, and no attempt was made to eliminate them. Appendix B contains a partial computer listing (every fifth value) of the net reaction rates for all species observed in flames III and IV.

From the appropriate species net reaction rates, rate coefficients for the following four reactions were calculated over a 100 K range in each flame:

$$H + CH_4 \rightarrow H_2 + CH_3 \quad (1)$$

$$H + O_2 \rightarrow OH + O \quad (2)$$

$$CO + OH \rightarrow CO_2 + H \quad (3)$$

$$CH_3 + O \rightarrow H_2CO + H \quad (4)$$

The details of these calculations have been discussed elsewhere (8, 10). The results are shown in figure 10, where log k_j is plotted versus (1/T K) for each reaction. The broken lines are from flame III, 1,500-1,600 K, and the solid lines are from flame IV, 1,725-1,825 K. Individual data points are shown only at the beginning and end of the range.

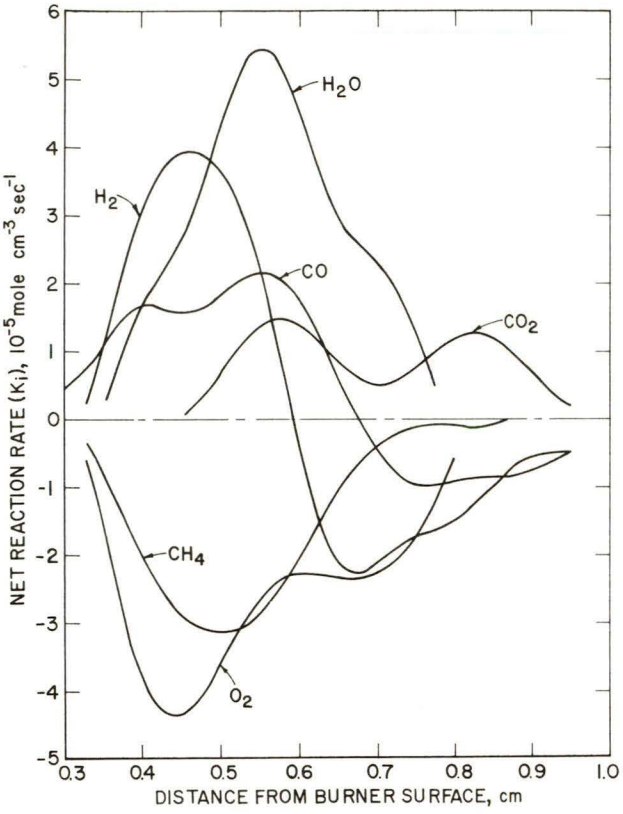

FIGURE 8. - Net reaction rate profiles for the major species of the uninhibited flame III.

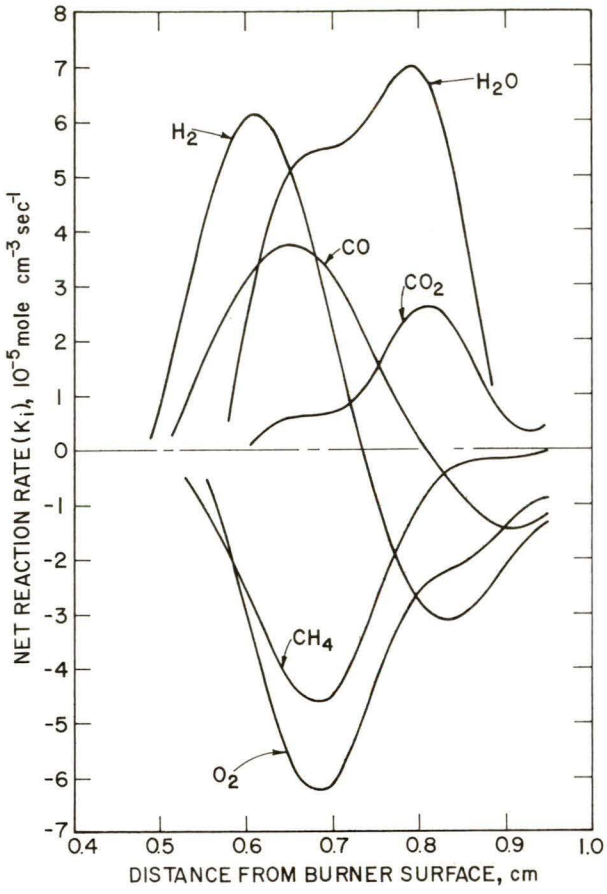

FIGURE 9. - Net reaction rate profiles for the major stable species unrelated to the inhibitor in the inhibited flame IV.

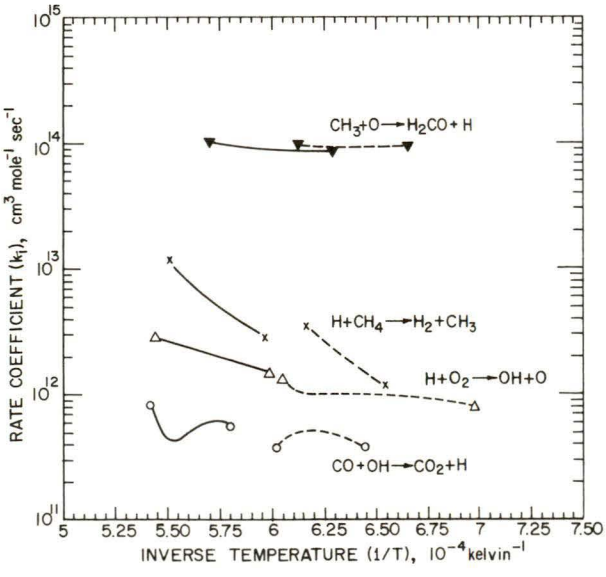

FIGURE 10. - Rate coefficients determined for elementary reactions occurring in methane flames. Dashed lines, results from uninhibited flame III; solid lines, results from inhibited flame IV.

The rate coefficients shown in figure 10 are similar in absolute value and temperature dependence to those obtained for the same reactions in earlier flame structure studies in our laboratory. There are several points to be made regarding these results. The first is in regard to observed temperature dependencies for $H+CH_4$ and $CO+OH$. It is the case that the rate coefficient for $H+CH_4$ exhibits curvature above 1,000 K (6, 15, 44). Thus, straight-line extrapolation of the rate coefficients in figure 10 to lower temperature will lead to erroneously low values of k for this reaction. A smooth extrapolation is not possible even over the 100 K gap that separates temperature ranges covered in these two flames. This reflects upon the precision with which the temperature dependence of a rate coefficient can be determined for a flame reaction when the calculation relies upon the net reaction rate for a species (CH_4) being consumed by other significant reactions ($CH_4 + OH \rightarrow H_2O + CH_3$). For the CO+OH reaction, we cannot discern any temperature dependence for the rate coefficient over the temperature range available in a single flame. However, the difference between the average values for k_3 in each flame gives an activation energy consistent with recent results for this reaction in this temperature range (50).

For flame IV, k_1 is calculated without consideration of the possible interfering reaction

$$Br + CH_4 \rightarrow HBr + CH_3 . \qquad (5)$$

This reaction has been proposed in some mechanisms of halocarbon inhibition as the source of regeneration of HBr, which is considered to be the principal radical scavenger. At the maximum rate of methane disappearance in flame IV, the temperature is 1,790 K, and reaction 5 can be calculated to account for about 6% of the observed net reaction rate for methane, using a rate coefficient determined in clean flames for k_1 (6) and extrapolating a value for k_5 from low-temperature studies (32). To the extent that this extrapolation is correct, reaction 5 is not important over the range of temperature for which k_1 is calculated in flame IV. Similar considerations apply to the calculation of k_4 in flame IV. If in the inhibited flame there are significant new routes for methyl radical disappearance, then k_4 will be lower than calculated here. One possible reaction is

$$CF_2 + CH_3 \rightarrow CH_2CF_2 + H, \qquad (6)$$

and consideration of this reaction would reduce k_4 by $\{k_6 (X_{CF_2}/X_O)\}$ at every point in flame IV. The ratio X_{CF_2}/X_O is 1 at 1,600 K and ~0.02 at 1,800 K. A reasonable estimate for k_6 is 10^{13} cm^3 mole^{-1} sec^{-1}, by analogy with a similar reaction involving methylene (33, 42), so k_4 might be lower than shown in figure 10 by as much as 12% at the low-temperature end of its range in the inhibited flame.

The relatively good temperature overlap of the rate coefficients shown in figure 10, reaction 1 notwithstanding, between clean and inhibited flames suggests that no significant changes in mechanism are occurring for the reaction of the species in question (CH_4, O_2, CO_2, CH_3) in the regions of the flame where they are reacting most rapidly. These reactions are simply delayed to higher temperatures when the inhibitor is present.

Comparisons Among Clean and Inhibited Flames

As with the flame containing 0.3% CF_3Br, the profiles shown in figures 4-7 are all shifted downstream relative to those of the clean flame (figs. 2-3). The shift is greater here, about 2 mm, than that observed in the 0.3% CF_3Br flame. The net reaction rate profiles for methane and oxygen (fig. 11) are also shifted to higher temperatures and are narrower in the inhibited flame. This effect was not as pronounced with the lower inhibitor concentration (7-8). These results are similar to those obtained by Wilson (52) for very lean CH_4-O_2 flames at 0.05 atm containing initially 1.88% HBr. Radicals could not be observed in that study, but a recent molecular beam investigation of a clean flame of similar composition and pressure (41) shows that OH and O are the dominant chain carriers and are first detected at about the same value of z. The concentration of hydrogen atom is at least four to five times smaller

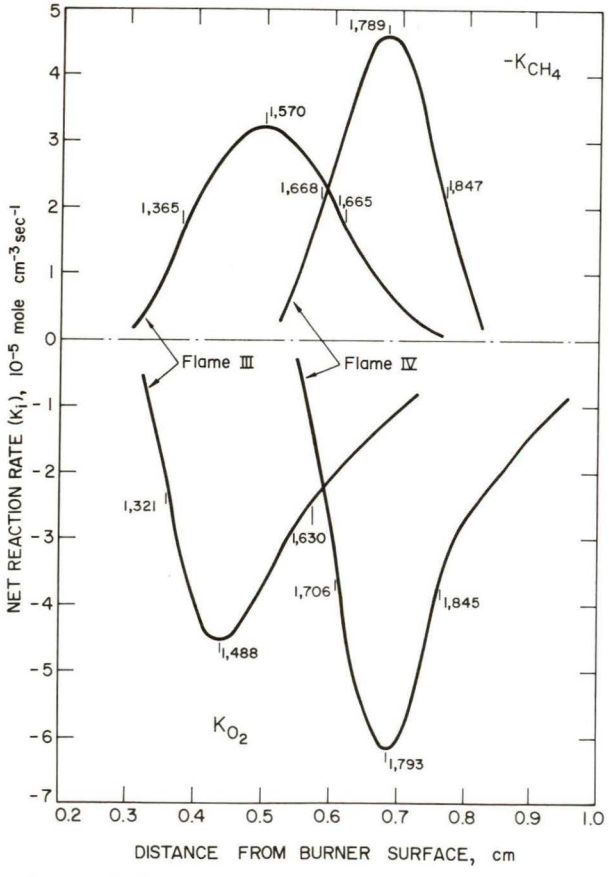

FIGURE 11. - Net reaction rate as a function of distance from the burner surface for methane and oxygen in flames III and IV. The temperature (K) is given at several values of z, cm.

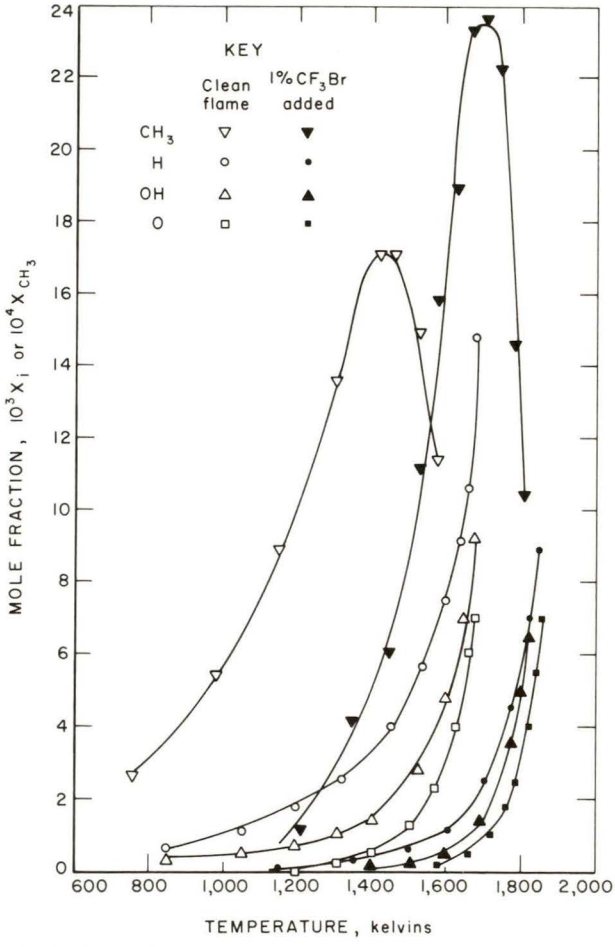

FIGURE 12. - Mole fraction of H, O, OH, and CH_3 as a function of temperature in the uninhibited flame III and the inhibited flame IV containing 1.1% CF_3Br. X_i is the mole fraction of H, O, or OH.

than [OH] and [O] in the lean flame.[6] In the nearly stoichiometric clean flames studied here, H is the chain carrier in greatest concentration everywhere in the flame, and it is observed earliest in the flame. The onset of OH and O is downstream of that for H, but the concentration differences among the three radicals are not as great in the stoichiometric as in the lean flame. Thus, even though different radical species predominate in the early part of these flames, the inhibitor has the same effect on the rates of disappearance of fuel and oxidant in each case. There are no data available that show directly the effect of CF_3Br or HBr on the radical species concentration in lean flames.

An examination (9) of the effect of CF_3Br on the concentrations of the principal radical species, H, O, and OH, reveals that, for flames containing 0.3% CF_3Br initially, only H atom concentrations are reduced at equivalent temperatures below ~1,600 K relative to the clean flame. At higher inhibitor concentration, 1.1% CF_3Br, all three radical concentrations are reduced in the low-temperature region of the flame, as shown in figure 12. The maximum radical concentrations are those expected assuming the characteristic H_2/O_2 reactions balanced at the final flame temperature. These maximum radical concentrations may increase or decrease (both were observed) when inhibitor is added to quenched flames.

The shifting of the primary reaction zone to higher temperature with the addition of inhibitor is responsible for the observed increase in peak methyl radical concentration in flame IV and also provides some insight into the nature of the reactions responsible for the decay of formaldehyde. The reactions forming methyl radical are reaction 1 and the analogous reaction of CH_4 with OH and, less importantly, with O. The rate coefficients for these reactions are temperature dependent. In the inhibited flame they occur at a higher temperature, and therefore CH_3 is formed at a faster rate than in the clean flames. The principal reaction removing CH_3, reaction 4, is not temperature dependent so its rate of decay is about the same in both flames. (At the peak X_{CH_3} in each flame, the concentration of O atoms is about the same.) The net effect is a higher peak concentration for CH_3 in the inhibited flame (fig. 12).

On the other hand, the product of reaction 4, formaldehyde, is reduced by nearly a factor of 4 in the 1.1% CF_3Br flame. A reduction of formaldehyde peak concentration was observed for the flame containing 0.3% CF_3Br (8) and in methane flames containing HBr (52). Since its formation rate is not substantially different between flames III and IV, the decrease in maximum $[H_2CO]$ must be caused by a greatly increased rate of decay in the inhibited flame. This implies a strongly temperature-dependent rate coefficient for the reactions responsible for that decay. It is possible to estimate that temperature dependence. At any given z, the net reaction rate for H_2CO is the difference between the overall rate of formation, K_f, and the overall rate of decay, K_d, of formaldehyde at that point in the flame

$$K_{H_2CO} = K_f - K_d .$$

[6] "Flame" in the context of this discussion refers to the preheat and primary reaction zones, to $0 < z \lesssim 1$ cm in the low-pressure studies.

If it is assumed that reaction 4 is the only significant process forming H_2CO, then

$$K_f = k_4[CH_3][O]$$

$$K_d = k_4[CH_3][O] - K_{H_2CO}. \qquad (C)$$

The decay processes are usually (22, 53) thought to be abstraction reactions

$$H(O,OH) + H_2CO \rightarrow H_2(OH,H_2O) + HCO, \qquad (7)$$

and there is evidence (29) that thermal decomposition reactions may be particularly important; for example,

$$H_2CO + M \rightarrow H_2 + CO + M. \qquad (8)$$

We can write

$$\left.\begin{array}{l} K_d = k_7[H_2CO]\Sigma[i] \quad i = H, O, OH \\ \text{or} \\ K_d = k_8[H_2CO][M] \end{array}\right\} \qquad (D)$$

where approximation is made that all of the abstraction reactions represented by reaction 7 have the same magnitude and temperature dependence. Substituting one of the equations D into equation C, it is possible to solve for k_7 or k_8 at any point in either flame. These calculations were carried out for both flames and spanned a temperature range of over 500 K.

The activation energy calculated for reaction 7 was 26 kcal $mole^{-1}$; for reaction 8 it was 44 kcal $mole^{-1}$. Such high activation energies suggest that reaction 8 or a similar thermal decomposition reaction is responsible for a significant part of the decay of formaldehyde, since the abstraction reactions have characteristically E_a ~2-4 kcal $mole^{-1}$ (16, 51). This is not to say that abstraction reactions do not occur. Indeed, the fact that the activation energy calculated for reaction 8 is rather higher than previously measured suggests that attributing all the H_2CO decay to reaction 8, as is done in the calculation described here, overestimates k_8. Our observations are consistent with a distribution between abstraction and thermal decomposition reactions first suggested by Peeters and Mahnen in their studies of lean CH_4-O_2 flames (41).

One model of flame inhibition proposes a zone of inhibition between the transport zone and the primary reaction zone of the flame (52). In this region of the flame, the inhibitor and/or its products of decomposition are thought to scavenge radicals efficiently and to compete with the normal chain-propagating or branching reactions, delaying those reactions until the temperature has increased to a point where the inhibiting reactions can no longer compete. Much of the data we have obtained is consistent with this model. Examples are the directly observed reduction of chain carrier concentrations in the low-temperature region of inhibited relative to clean flames, the early reaction of the inhibitor molecule relative to fuel, and the shifting to

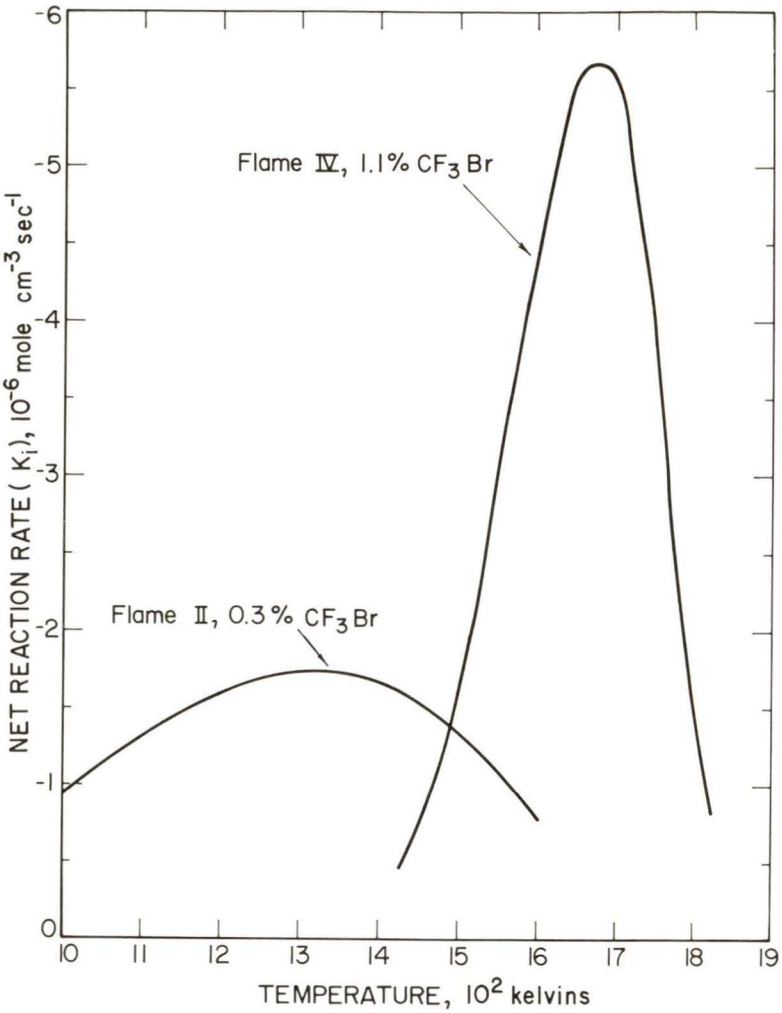

FIGURE 13. - Net reaction rate for the inhibitor as a function of temperature for two nearly stoichiometric methane flames containing initially different amounts of CF_3Br.

higher temperatures of the net reaction rate of fuel and oxidant in the presence of inhibitor. However, the behavior of the inhibitor in the 1.1% CF_3Br flame relative to the 0.3% flame is not similarly consistent. In each case, the inhibitor begins to react and achieves its maximum rate of decay earlier (at lower z and T) than methane, but the CF_3Br reacts more rapidly at significantly higher temperature in the 1.1% flame than in the 0.3% flame. Figure 13 shows K_{CF_3Br} as a function of temperature in flames II and IV. Table 2 lists the temperatures at which the maximum rates of decay occur for methane and CF_3Br in all four flames examined. Flames I and III differ initially in mass flow rate only and hence the difference in final flame temperature (28). The temperature at which CH_4 disappears most rapidly reflects the difference. Flames II and IV also differ in initial inhibitor concentration. The final flame temperature is 50 K higher for IV, but the maximum net reaction rate for CF_3Br occurs at a temperature 365 K higher in IV than II. The shift to higher temperature and narrowing of K_{CF_3Br} in flame IV relative to flame II (fig. 13) is like that of methane in the inhibited relative to the clean flames. The maximum rate of decay of CF_3Br in flame IV is greater than in flame II, owing to the greater initial CF_3Br concentration in the former.

TABLE 2. - Temperature for maximum rate of decay of fuel and inhibitor in 0.042 atm, nearly stoichiometric CH_4-O_2-Ar flames[1]

Flame	Initial [CF_3Br], %	T_{final}	T at $\lvert K_{CH_4} \rvert_{max}$	T at $\lvert K_{CF_3Br} \rvert_{max}$
I.....	0	1,868	1,640	-
III.....	0	1,781	1,570	-
II.....	0.3	1,911	1,660	1,310
IV.....	1.1	1,966	1,790	1,675

[1]All temperatures are in kelvins.

With increasing inhibitor concentration, the zone of inhibition, if that idea is at all applicable, is also shifted to higher temperature, and the reaction of the inhibitor itself is also delayed. At equivalent temperatures the concentrations of H, O, and OH are smaller than in flame II (9), and the observed delay in inhibitor decay seems to be a consequence of this reduction in radical concentration. The implication is that of the several possible reactions that can be written to account for the observed reduction of radical concentration in the low-temperature region of the flame, those between CF_3Br and radicals, for example,

$$H + CF_3Br \rightarrow HBr + CF_3 , \qquad (9)$$

are not the most important. Reaction 9 does occur and is still a significant reaction destroying CF_3Br in the flame, as will be discussed presently, but it is delayed to higher temperatures, just as reaction 1 is.

Disappearance of CF_3Br

In the 0.3% CF_3Br flame, it was found that at the maximum rate of disappearance of CF_3Br, thermal decomposition could account for, at most, 8% of the decay rate. The rate coefficient, k_{td}, given by Benson and O'Neal (3) was used. Reaction with H atom to give HBr and CF_3 was responsible for the disappearance of CF_3Br, and a rate coefficient could be calculated. The result was given by $2.2 \times 10^{14} \exp(-9{,}460/RT)$ for $700 < T < 1{,}550$ K. In the flame containing 1.1% CF_3Br initially, at the maximum decay rate for CF_3Br, the predicted rate of thermal decomposition, k_{td} (again using Benson and O'Neal's rate coefficient), is nearly 10 times greater than the observed net reaction rate, $\lvert K_{td} \rvert_{B\&O} = 10 \lvert K_{CF_3Br} \rvert_{max}$.

The value for the thermal decomposition rate coefficient recommended by Benson and O'Neal is from an RRK calculation and represents an attempt to calculate the limiting high-pressure value. The only experimental value for k_{td}, reported by Sehon and Szwarc (45), is more than a factor of 10 lower than Benson and O'Neal's. Thus, at the temperature of interest, using Sehon and Szwarc's number, we might conclude that CF_3Br disappears by thermal decomposition.

Hydrogen atoms are present in the region of flame IV over the temperature range in which CF_3Br disappears. Although the H atom concentration at any given temperature below the maximum temperature is lower than in flame III,

these concentrations are not negligible. At the maximum CF_3Br decay rate, if we assume the abstraction reaction alone is responsible for the decay, we calculate a value of $k_9 = 1.6 \times 10^{13}$ cm^3 $mole^{-1}$ sec^{-1}, T = 1,666 K. The number agrees well with the value (1.3×10^{13}) extrapolated using the expression given earlier.

Thus assigning the decay of CF_3Br either to thermal decomposition or to H atom abstraction would yield values for the rate coefficients for these reactions that are consistent with what is known about either reaction. This holds over the range of CF_3Br decay for which $1,600 \leq T < 1,800$ K.

It is reasonable to suppose that, in this flame, CF_3Br is consumed by both abstraction and thermal decomposition reactions. If we assume that the abstraction reaction occurs with the rate coefficient measured in flame II, we can estimate a CF_3Br decay rate due to abstraction. Where the observed CF_3Br decay rate is greater than the calculated abstraction rate, we assign the difference to thermal decomposition. For $T \geq 1,670$ K this difference is positive and the thermal decomposition rate constant, expressed as a first-order coefficient, is the solid line shown in figure 14. At temperatures lower than 1,670 K, the abstraction reaction predicts a greater rate of CF_3Br decay than observed, and so a meaningful k_{td} cannot be calculated. At 1,600 K, for example, the observed K_{CF_3Br} is 75% of that required if the abstraction and thermal decomposition were occurring, the latter proceeding at the rate required by extrapolating the solid line in figure 14 to 1,600 K. On the basis of this analysis, thermal decomposition accounts for about 50% of the CF_3Br disappearance rate at its maximum in flame IV and at higher temperature.

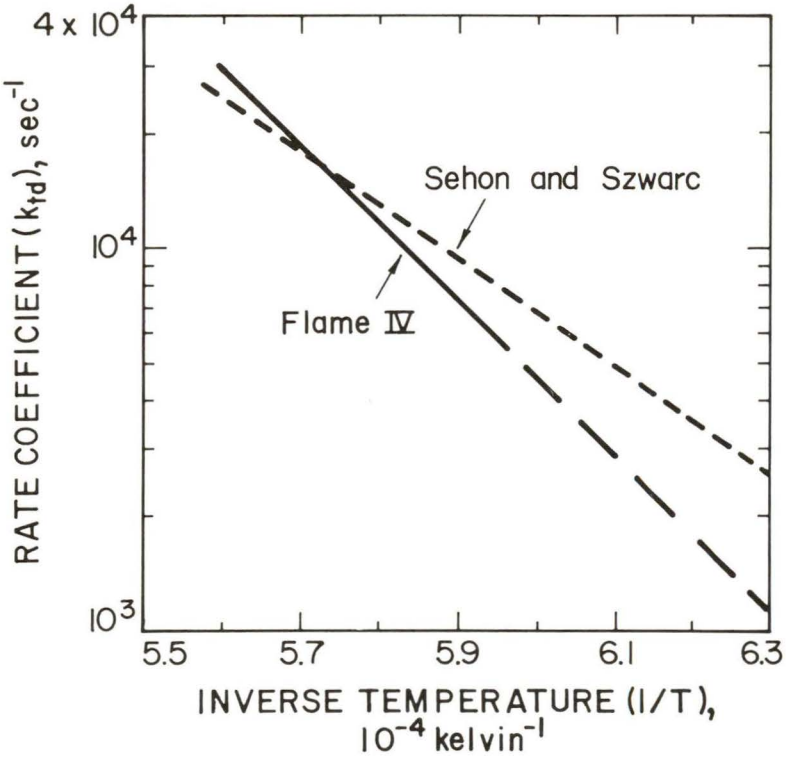

FIGURE 14. - Rate coefficient for thermal decomposition of CF_3Br, expressed as first order, calculated assuming Br atom abstraction occurs with the rate constant previously determined (8). Solid line, flame IV; dashed line from reference 45.

We expect (10) to be able to use net reaction rate curves (fig. 13) to about $1/2|K_{CF_3Br}|_{max}$, $1,550 \leq T \leq 1,780$ K. The fact that we cannot utilize the low-temperature portion of the K_{CF_3Br} is an inconsistency that is ultimately due

to experimental limitations of these flame data, to the errors in modeling thermal diffusion noted earlier, to error in determining the absolute value of H atom concentration, particularly at low values of z, and to possible limitations in the curve-smoothing operation for reactant-type profiles at low z values. All of these possible sources of error diminish in magnitude with increasing values of z and T.

The dashed line in figure 14 is the expression for k_{td} of Sehon and Szwarc (45), extrapolated to flame temperature. The conditions of Sehon and Szwarc's experiment were 5-20 torr and 1,020-1,090 K. From Benson and O'Neal's calculations, it is likely that these conditions are well into the pressure-falloff region for CF_3Br decomposition. The pressure here is higher, 32 torr, but so is the temperature, and our conditions are also probably well into the pressure-falloff region. In absolute value, our calculated rate coefficient for thermal decomposition is not very different from extrapolation of Sehon and Szwarc's measurements, and both are at least an order of magnitude lower than the computed high-pressure limiting value.

As in previous work (7), reactions of CF_3Br with O and Br atoms were found to be negligibly important. Abstraction by methyl radical to give CH_3Br accounted for 10% to 30% of the decay rate of CF_3Br below 1,700 K. The reaction was considered, quantitatively, in making the calculations for the contribution of thermal decomposition. The reverse reactions, forming CF_3Br, are also unimportant in the flame.

Compositions and Kinetic Analyses of Inhibitor-Related Species

When 1.1% CF_3Br is added to a methane flame, a number of brominated and fluorinated species are observed. They are Br_2, CH_3Br, HBr, CH_2CF_2, CF_2, CF_3H, F_2CO, HF, and the Br atom. Figures 6 and 7 show the concentration profiles for these species. The first six are relatively short-lived intermediates, F_2CO is a long-lived intermediate, and HF and Br have the appearance of "products" in low-pressure flames. The net reaction rate profiles calculated according to equations A and B for all the inhibitor-related species except Br atom are illustrated in figures 15-17. The rate profiles shown are plots of the net reaction rates listed in appendix B with local variations removed. Some concepts that are important in understanding the flame as a chemically reacting system are illustrated by these figures. From figure 7 it appears that molecular Br_2 is formed at low values of z in the flame, and this is confirmed by its net reaction rate in figure 17. However, in general, it is not possible to deduce from the spatial order of observation of the species in the flame, the spatial order in which they are formed in the flame. For example, HF (fig. 7) is observed in appreciable amounts at $z \sim 0.4$ cm, and its maximum rate of production is at $z \sim 0.6$ cm (fig. 15). The HF observed at low z is due entirely to diffusion induced by the large concentration gradient of HF. This is true of all of the inhibitor-related species except Br_2 and may be observed by comparing the onset of the appropriate profiles of figures 6 and 7 with those of figures 15-17.

With the possible exception of Br_2 and CF_3H, the kinetic steady state approximation ($d[i]/dt \sim 0$ relative to some other rate process) does not apply

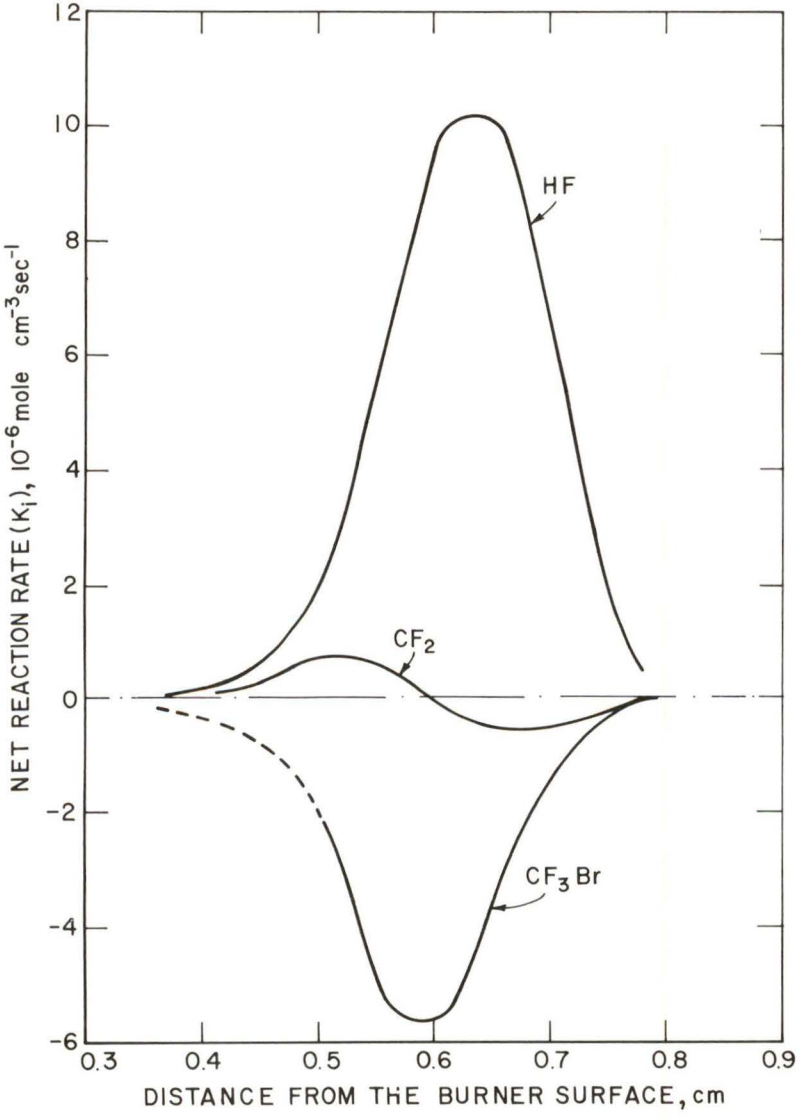

FIGURE 15. - Net reaction rate profiles for HF, CF_2, and CF_3Br in flame IV.

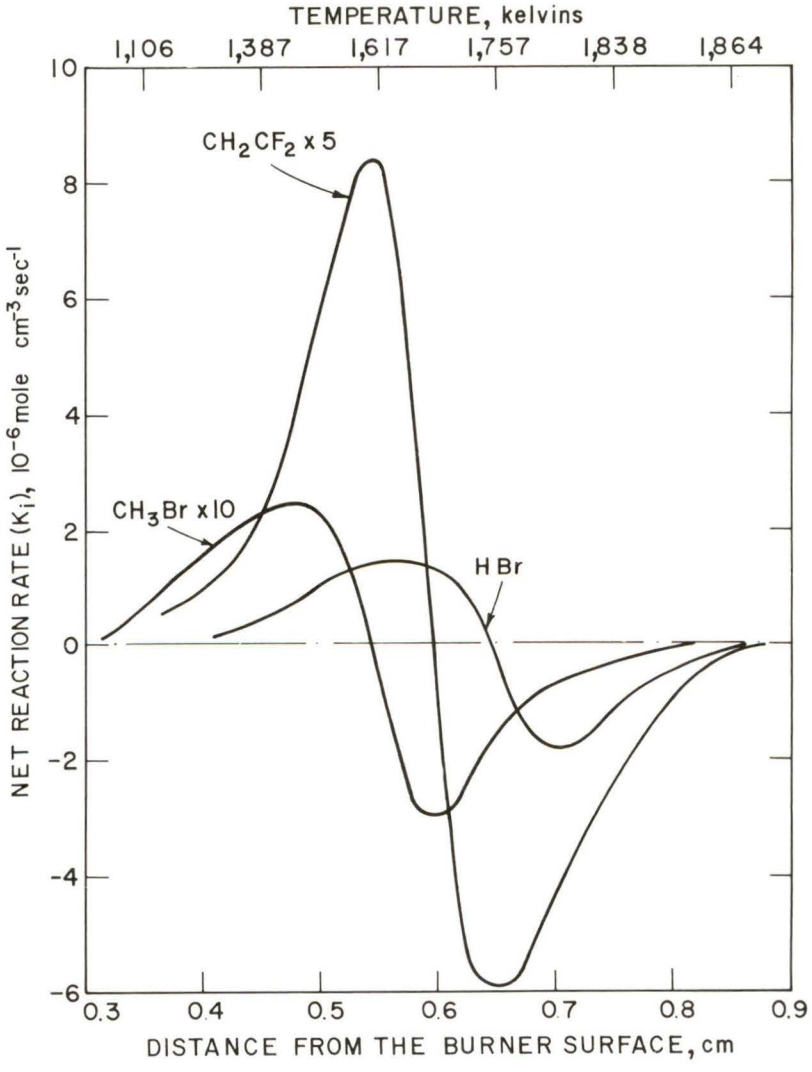

FIGURE 16. - Net reaction rate profiles for CH_3Br, CH_2CF_2, and HBr in flame IV.

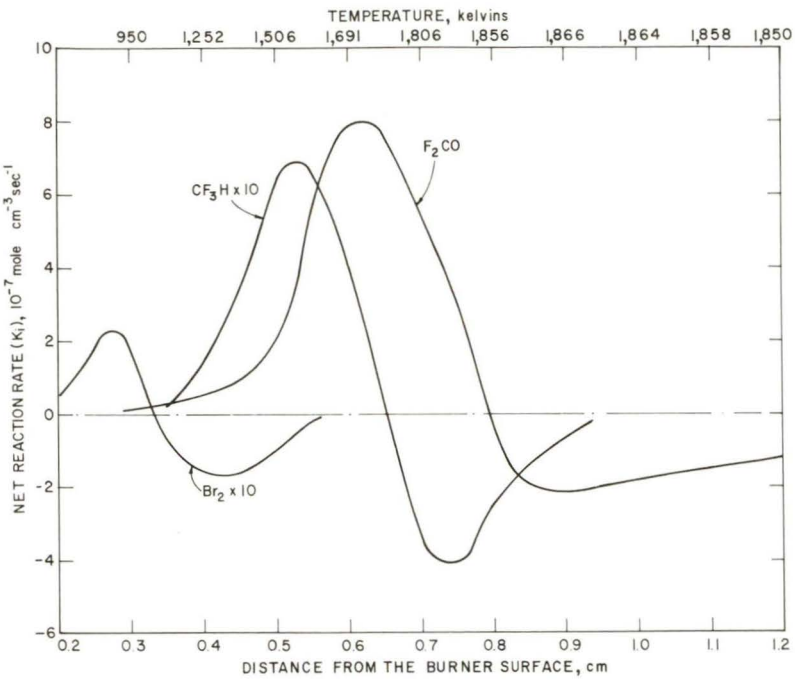

FIGURE 17. - Net reaction rate profiles for Br_2, CF_3H, and F_2CO in flame IV.

to any of the intermediate species related to the decay of CF_3Br. The simplification afforded by this approximation in other complex reaction systems is not generally available in flame analyses.

The species formed earliest in the flame are, in addition to Br_2 (870 K), CH_3Br (1,448 K) and CF_2 (1,538 K), followed by CF_3H (1,569 K), CH_2CF_2 (1,598 K), and HBr (1,634 K); the temperature at which the maximum net reaction rate is observed is given in parentheses. The F_2CO (1,720 K) and HF (1,731 K) are clearly later intermediates, well separated from the other species related to the decay of CF_3Br. The dashed part of the net reaction rate curve for CF_3Br (fig. 15) is calculated from the sum of the observed net reaction rates of species formed directly as a result of the reaction of CF_3Br.

There are some differences in the relative order of appearance of these species between flame IV and flame II, containing initially 0.3% CF_3Br (7). In that flame the maximum F_2CO appearance rate preceded that for HF, and both the HF and HBr maxima occurred at about the same value of z. The temperature profiles are different between these two flames, so that the place at which a given species reaches a maximum or a minimum in K_i will depend upon the temperatures and the temperature dependencies of all the reactions contributing to the formation and decay of the species. The difference in the relative position of HBr between flame II and flame IV may be a reflection of the differences in the decay mechanism for CF_3Br between the two flames. As previously noted, in flame II, decay is predominately via the abstraction reaction $H+CF_3Br \rightarrow HBr+CF_3$; in flame IV, the thermal decomposition reaction giving Br and CF_3 is also important. Thus the reaction $Br+H_2 \rightarrow HBr+H$ may be more important in the overall rate of formation of HBr at low temperature in flame IV than in flame II.

The individual net reaction rate, K_i, determined by equation B is the collective effect of all the reactions forming and all the reactions consuming the species i. When the reactions responsible for the production and decay of a given species are known, particularly when a single reaction path dominates, it is straightforward to calculate a rate coefficient for the dominant reaction from the complete microstructure data, as is done for reactions 1-4. When the mechanisms are only partially known, as is the case here, the

procedure is to propose reactions that could explain the observation of a particular species. When rate coefficients for these reactions have been measured in other systems, or can be reasonably estimated, it is possible to calculate the value of K_1 to be associated with each reaction. Comparison with the observed K_1 gives an indication of the importance of the proposed reaction. Rate coefficients that are consistent with the proposed mechanism can be calculated for individual reactions if there is sufficient kinetic data available for most of the other reactions in the scheme. Rate coefficients so determined are frequently the only available quantitative data for the reactions at elevated temperature. The analyses that follow are the result of applying the procedure outlined above to inhibitor-related species in flame IV.

CH_3Br and CF_3H.--The reactions found to be significant in the formation and decay of CH_3Br in the inhibited flame over the temperature range 1,250-1,600 K follow:

Formation	$CH_3+CF_3Br \rightarrow CH_3Br+CF_3$	(10)
	$CH_3+Br_2 \rightarrow CH_3Br+Br$	(11)
Decay	$CH_3Br+H(OH) \rightarrow HBr(HOBr)+CH_3$	(12-13)
	$CH_3Br+Br \rightarrow HBr+CH_2Br$	(14)
	$CH_3Br \rightarrow CH_3+Br$	(15)

Reactions 11 and 14 are relatively minor contributors to K_1, so that even if the absolute concentration of Br_2 is in error by an order of magnitude, the rate coefficient calculated for CH_3Br formation by reaction 10 would not be significantly different. Reactions of CH_3Br with O, CF_3, and CH_3 are negligibly slow here. To the extent that quantitative information is available for the reverse reaction, either from measurement of the reverse or from calculations using equilibrium constants and the rate coefficient of the forward reaction, the reverse reactions are also slow.

A rate coefficient, k_{10}, for reaction 10 over the temperature range cited may be calculated by quantitatively taking into account the contribution of the other reactions (7). The results are shown in figure 18. Shown also are the earlier results from the flame initially containing 0.3% CF_3Br. The temperature range over which this rate coefficient was determined in that flame was 650 to 1,250 K, and the values below 900 K depended importantly upon an estimated concentration of Br_2 in that flame. The points shown in figure 18 are for $900<T<1,600$ K, and the value 5.8×10^{12} $\exp(-4,200/RT)$ cm^3 $mole^{-1}$ sec^{-1} for k_{10} from both flames is a better estimate for this rate coefficient than that obtained from either flame separately.

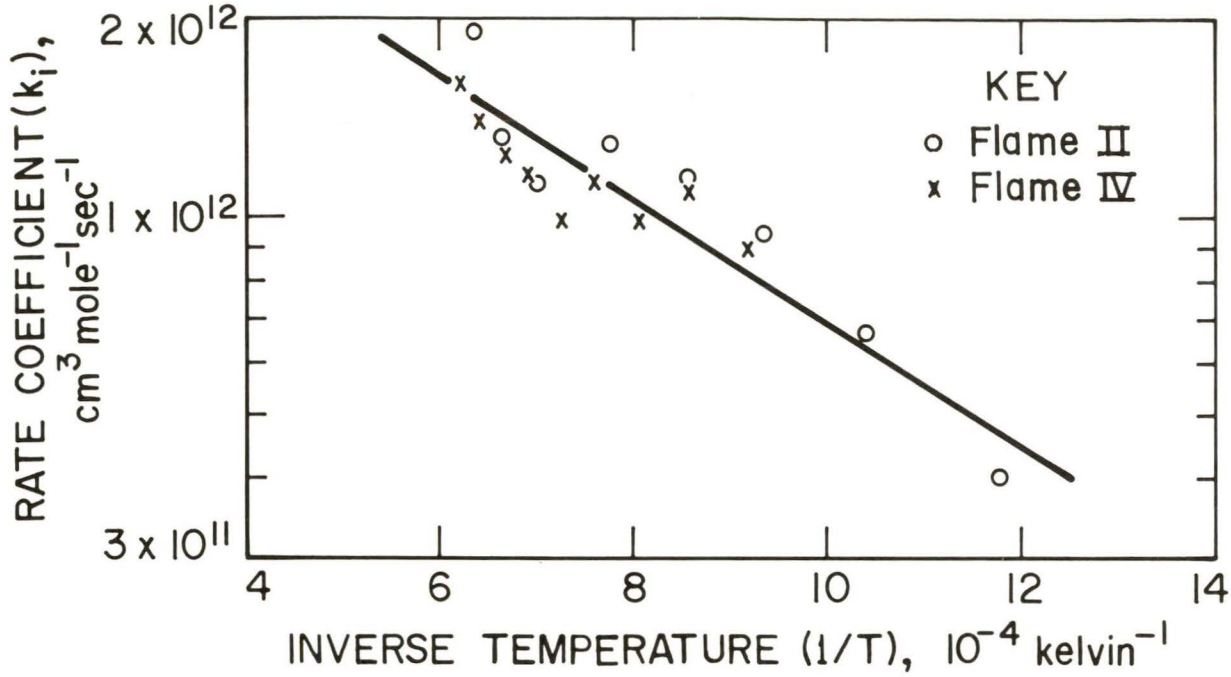

FIGURE 18. - Rate coefficient for the reaction $CH_3+CF_3Br \rightarrow CH_3Br+CF_3$ as a function of temperature as determined from analysis of flame II and flame IV. The Arrhenius expression for k is 5.8×10^{12} exp(-4,200/RT) cm^3 mole^{-1} sec^{-1}, $900<T<1,600$ K.

CF_3H is the only observed inhibitor-related species that contains the CF_3 group intact. We use its net reaction rate, with the assumption that it is formed by H atom abstraction reactions between CF_3 and various hydrogen-containing species in the flame, to calculate a profile for CF_3 in the flame (11). A formation reaction not considered earlier, $CF_2+HF \rightarrow CF_3H$, is about two orders of magnitude slower than the observed rate of CF_3H formation and is therefore negligible. In the calculation a value for the rate coefficient analogous to that recommended for insertion by HBr and HCl was used (1, 17).

The decay reaction for CF_3H is relatively slow, since CF_3H is next to the last to disappear (F_2CO is last) of the intermediates associated with the inhibitor (fig. 17). Several reactions may be important in the decay:

$$CF_3H+H(O,OH) \rightarrow H_2(OH,H_2O)+CF_3 \quad (16)$$

$$CF_3H \rightarrow CF_2+HF \quad (17)$$

$$Br+CF_3H \rightarrow HBr+CF_3 \quad (18)$$

$$CH_3+CF_3H \rightarrow CH_4+CF_3 \quad (19)$$

Reactions 16, 18, and 19 are the reverse of important formation reactions, and using rate coefficients from standard sources (32, 48), reactions 18 and 19 are found to be too slow to be important sources of decay of CF_3H. At the position of maximum decay, reaction 16, with H atoms, accounts for only ~8% of the observed decay rate. Since [H]~[OH] here and [O] is about half that, at best, radical abstraction reactions, assuming them all to be equally fast, can account for only 20% of the observed net reaction rate. The thermal decomposition reaction 17 is of primary importance in the disappearance of CF_3H, and we calculate a value for k_{17}, expressed as a first-order rate constant, of $(6\pm1)\times10^3$ sec^{-1} at T = 1,845 K. This result is about seven times lower than suggested by the only other value reported in the literature (49). That datum was from a shock tube experiment in which the average conditions of measurement were 3,000 torr and 1,400 K. The authors considered the reaction to be into the falloff region under those conditions, and the flame conditions here are even farther from the high-pressure limit. Expressed as second order, $CF_3H+M \rightarrow CF_2+HF+M$, the rate coefficient is 2×10^{10} cm^3 $mole^{-1}$ sec^{-1} at 1,845 K, where M is any other molecule in the flame.

The CF_2, CH_2CF_2, F_2CO, HF Axis.--The four named species are linked together by the fact that reactions forming some of them consume others, and while we can estimate rate coefficients for these reactions based upon the behavior observed for the net reaction rate of individual species, their behavior is related. For this reason we discuss the kinetic analyses of these species together. Table 3 lists the reactions that are pertinent to their formation and decay in the flame, together with the literature rate coefficients and references to the literature on the reactions.

The reactions responsible for the formation and decay of CF_2, as determined from analyses of the net reaction rate profile for CF_2, have been published (11). Some new information from considerations of $K_{CH_2CF_2}$ has implications for the estimated rate coefficients of the CF_2 reactions and will now be discussed.

Observation of CF_2 in flame IV suggests for the formation of CF_2CH_2 the reaction

$$CF_2+CH_3 \rightleftarrows (CF_2CH_3)^* \rightarrow CF_2CH_2+H \qquad (20)$$

by analogy to the reaction between (triplet) methylene and methyl radical (33, 42). This is in addition to the reactions proposed earlier (7),

$$CF_3+CH_3 \underset{(-21)}{\overset{(21)}{\rightleftarrows}} (CF_3CH_3)^* \xrightarrow{(22)} CF_2CH_2+HF.$$

TABLE 3. - Reactions of the principal fluorocarbon species in inhibited flames

Reaction	Literature rate coefficient, cm^3 $mole^{-1}$ sec^{-1}	Reference	Remarks
(20) $CF_2+CH_3 \rightleftarrows (CF_2CH_3)^* \rightarrow CF_2CH_2+H$...	-	42	By analogy to $^3CH_2$ reaction for which $k = (3\text{-}6)\times10^{13}$ cm^3 $mole^{-1}$ sec^{-1}.
(21-22) $CF_3+CH_3 \rightleftarrows (CF_3CH_3)^* \rightarrow CF_2CH_2+HF$	$k_{13} = 6.8\times10^{13}$ (440 K)	31, 43, 47	-
(23) $CF_3+H \rightarrow CF_2+HF$.....	5×10^{13} (1,540 K) - 2×10^{14} (900-1,300 K)	11, 46	-
(24) $CF_3H \rightarrow CF_2+HF$.....	1.2×10^{12} exp(-63,000/RT) sec^{-1}	49	Reaction conditions likely to be in the pressure falloff region.
(25a) $CH_2CF_2+O \rightarrow F_2CO+CH_2$.....	4×10^{13} exp(-3,200/RT)	7, 27, 37, 38	-
(25b) $\rightarrow H_2CO+CF_2$.....			
(26) $CF_2+H \rightarrow CF+HF$.....	10^{13} (1,800 K)	11	-
(27a) $CF_2+O \rightarrow CO+F+F$.....	-	25, 39	A rate coefficient of $(1\text{-}5)\times10^{13}$ was estimated for these reactions collectively in reference 11.
(27b) $\rightarrow F_2CO$.....	-	2	
(27c) $\rightarrow FCO+F$.....	-	30	
(28a) $CF_2+OH \rightarrow CO+HF+F$.....	$(1\text{-}3)\times10^{13}$ (1,800 K)	11	-
(28b) $\rightarrow F_2CO+H$.....			
(29a) $CF_2+O_2 \rightarrow F_2CO+O$.....	2×10^{13} exp(-26,500/RT)	30	-
(29b) $\rightarrow CO+2F+O$.....	-	-	Endothermic.
(30) $CF_3+O_2 \rightarrow F_2CO+OF$.....	-	26	By analogy to CH_3 reaction for which $k = 1.2\times10^{12}$ exp(-12,500/RT) cm^3 $mole^{-1}$ sec^{-1}.
(31) $CF_3+O \rightarrow F_2CO+F$.....	-	7, 41	By analogy to CH_3 reaction for which $k\sim10^{14}$ cm^3 $mole^{-1}$ sec^{-1}.
(32) $CF_3+OH \rightarrow F_2CO+HF$.....	-	7, 19	By analogy to CH_3 reaction for which $k = 4\times10^{12}$ cm^3 $mole^{-1}$ sec^{-1}.

*Denotes a vibrationally excited molecule.

Reaction 20 was not considered in the analyses of flame II. In that flame it was estimated that $X_{CF_3} \leq 10^{-4}$, from our inability to detect this radical. From the current data[3], the maximum mole fraction of CF_3 in flame II was more like 10^{-5}, and a rate coefficient calculated for reaction 21 from that data is an order of magnitude higher than reported earlier. The rate coefficient from the present calculation is $>2\times10^{14}$ cm^3 mole^{-1} sec^{-1}, and k_{21} would be greater to the extent that reactions 21, -21 are in the pressure falloff region for the conditions of that flame. A similar calculation, in which reaction 20 was ignored entirely, was performed for flame IV and gave $k_{21}>5\times10^{14}$ cm^3 mole^{-1} sec^{-1} at 1,435 K. A value of 6.8×10^{13} cm^3 mole^{-1} sec^{-1} is recommended for k_{21} (24). Since this value is nearly gas kinetic, and if anything, likely to be smaller at high temperature, it is unreasonable to assign the formation of CH_2CF_2 solely to the sequence of reactions 21-22.

The literature value for the rate coefficient of reaction 21, the measured concentration of CF_2, and the calculated concentration of CF_2 were used to account for the contribution of the sequence of reactions 21-22 to the net rate of formation of CH_2CF_2. In the temperature range $1{,}300<T<1{,}600$ K, CH_2CF_2 is being formed (fig. 16), and decay reactions are assumed to be unimportant. A value for k_{20} was calculated over this temperature and found to be temperature insensitive at 2×10^{13} cm^3 mole^{-1} sec^{-1}. Inclusion of the decay reactions for CH_2CF_2, to the extent that their rate coefficients are known (11), does not significantly change this number below 1,600 K. At the point in the flame where CH_2CF_2 is being formed at a maximum rate, reaction 20 accounts for ~80% of that formation rate; reactions 21-22 account for, at most, 20%. The same mechanism may be reasonably applied to flame II (7). Previously we supposed only reactions 21 and 22 were important in flame II (7). We did not look for the CF_2 radical in that flame and observed it for flame II subsequent to the experiments on flame IV (11).

In analyzing the net reaction rate profile for CF_2 (11), the reaction between CF_2 and CH_3 was considered to give HF and the $CFCH_2$ radical, an endothermic reaction that was neglected as slow. When reaction 20 is added to the decay scheme for CF_2 using the rate coefficient determined in the preceding analysis, we calculate rate coefficient for other reactions forming and consuming CF_2 that are higher than those reported earlier (11). The reactions (table 3) forming CF_2 are 23, 24, and 25b; the reactions consuming CF_2 are 20, 26, 27, and 28. A rate constant of 8×10^{14} cm^3 mole^{-1} sec^{-1} for reaction 23 is consistent with this mechanism. This number is a factor of four greater than that calculated ignoring reaction 20 and corresponds to the reaction occurring essentially at every collision. Reactions 26-28 have rate coefficients two to three times greater than previously estimated, depending upon which radical is assumed to dominate the decay. If the reactions between CF_2 and H, O, and OH are equally fast, then the rate coefficient for those reactions at $1{,}800\pm30$ K is 3×10^{13} cm^3 mole^{-1} sec^{-1}.

Carbonyl fluoride may be produced by several different reactions:

$$CF_2+O \rightarrow F_2CO \qquad (27b)$$

$$CF_2+OH \rightarrow F_2CO+H \qquad (28b)$$

$$CF_2+O_2 \rightarrow F_2CO+O \quad (29a)$$

$$CF_3+O_2 \rightarrow F_2CO+OF \quad (30)$$

$$CF_3+O \rightarrow F_2CO+F \quad (31)$$

$$CF_3+OH \rightarrow F_2CO+HF \quad (32)$$

$$CH_2CF_2+O \rightarrow F_2CO+CH_2 \quad (25a)$$

The net reaction rate profile for F_2CO (fig. 17) shows an unusually long upstream foot. Although most of the F_2CO is formed at higher temperatures, it is being formed even at temperatures as low as 1,100 K in the flame. K_{F_2CO} begins to increase rapidly where O atoms are observed in the flame, and the most important reactions forming F_2CO are those involving O atoms. Below about 1,375 K, the concentration of oxygen atoms is zero, and reactions 27b, 31, and 25a may be neglected. The contributions of reactions 30 and 32 were estimated by assigning to them the rate coefficients of analogous methyl radical reactions (7, 19) with the result that both reactions are negligibly slow here. Reaction 29a is of minor importance, contributing at most 20% of the observed net reaction rate of F_2CO at temperatures below 1,375 K. The reaction principally responsible for F_2CO formation in the absence of oxygen atoms is reaction 28b, $CF_2+OH \rightarrow F_2CO+H$. Using K_{F_2CO} for $1{,}090<T<1{,}375$ K, the rate coefficient for reaction 28b is calculated to be $(5\pm1)\times10^{12}$ cm^3 $mole^{-1}$ sec^{-1}, where the limits show precision only.

Previously we calculated 3×10^{13} cm^3 $mole^{-1}$ sec^{-1} for CF_2+(OH, O, or H), assuming equal rate coefficients for each radical (11). The present result is consistent in that several reactions for CF_2 with O and OH, including reaction 28b, were considered together in the CF_2 analysis.

For $1{,}495<T<1{,}780$ K, where F_2CO is being formed most rapidly and the oxygen atom concentration is not zero, the principal formation reactions are CF_2+O (27b) and CH_2CF_2+O (25a). The reactions involving CF_3, including reaction 31, together account for about 20% of the observed K_{F_2CO} over this temperature range. Reaction 29a, CF_2+O_2, diminishes in importance, contributing at most 5% to K_{F_2CO}. We account for reaction 28b using the rate coefficient determined at lower temperature. We cannot, from the F_2CO analysis, determine which of the two reactions, 27b or 25a, dominates. Assigning the formation to reaction 25a alone suggests a rate constant for this reaction of 1×10^{13} cm^3 $mole^{-1}$ sec^{-1}, in agreement with a similar analysis for flame II (7). Assigning the formation to reaction 27b alone requires a rate coefficient of 2×10^{13} cm^3 $mole^{-1}$ sec^{-1} for that reaction. This last number is consistent with the estimate made from the CF_2 net reaction rate analyses.

Reaction 27b, CF_2+O, is spin disallowed and, presumably, slow. Bauer (2), from shock tube studies of the oxidation of perfluoroethylene, suggests that this reaction has a rate constant very much larger than that for the reaction of CF_2 and molecular oxygen (reaction 29a). The rate coefficient for that reaction at the midpoint of the temperature range considered here, 1,635 K, is 5.7×10^{9} cm^3 $mole^{-1}$ sec^{-1} (30).

Reaction 25a, $CH_2CF_2+O \rightarrow F_2CO+CH_2$, is spin allowed and has been identified as occurring in the room temperature photolysis of NO_2 and $CF_2 = CXY$ mixtures, where X and Y are either F, H, Cl, or Br (37). Those results suggest, however, that reaction 25b (table 3) rather than reaction 25a is the dominant reaction path for the interaction of CH_2CF_2+O. If that is also true at flame temperatures (and we cannot distinguish directly between the two paths here), then not only is reaction 27b the most important F_2CO formation route in the flame, but the results of the reassessment of the K_{CF_2} analyses discussed earlier represent upper limit values for the rate coefficients involved. The latter follows from the fact that reaction 25b represents a formation reaction for CF_2 whose occurrence mitigates the effect of consumption reaction 20 to the extent that their rates are similar.

There are 10 reactions in table 3 that may lead either directly to HF or to F atoms which we assume rapidly abstract a hydrogen atom from other flame species to yield HF. These reactions are

$$CF_3+CH_3 \rightarrow \ldots \rightarrow CF_2CH_2+HF \qquad (21\text{-}22)$$

$$CF_3+H \rightarrow CF_2+HF \qquad (23)$$

$$CF_2+O \rightarrow CO+F+F \qquad (27a)$$

$$\rightarrow FCO+F \qquad (27c)$$

$$CF_2+OH \rightarrow CO+HF+F \qquad (28a)$$

$$CF_3+O \rightarrow F_2CO+F \qquad (31)$$

$$CF_3+OH \rightarrow F_2CO+HF \qquad (32)$$

$$CF_2+H \rightarrow CF+HF \qquad (26)$$

$$CF_3H \rightarrow CF_2+HF \qquad (24)$$

$$CF_2+O_2 \rightarrow CO+2F+O \qquad (29b)$$

Reaction 29b can be eliminated from consideration since it is endothermic and its rate will be slower than for exothermic reaction 29a (table 3). The rate coefficient for 29a has been determined (30), and the rate of this reaction is negligibly slow with respect to the observed K_{HF} everywhere in the flame.

Because of the number of reactions leading to HF and the paucity of literature rate data for these reactions, we cannot eliminate or account for enough of them to calculate independent rate constants for the others from the observed K_{HF}. We can, however, learn something about the magnitude of the rate coefficients for the reactions by comparison with the decay of CF_3Br. In this analysis, we can also use rate coefficients previously determined from the net reaction rates of other species to make decisions about which of these reactions are most important in producing HF in different regions of the flame.

If the reactions yielding HF from CF_3Br were very fast relative to the decay rate of CF_3Br, we would expect to observe three HF molecules produced rapidly for every CF_3Br molecule that decays and that

$$-(K_{HF})_{max} \sim 3\ (K_{CF_3Br})_{min}.$$

We find that

$$-(K_{HF})_{max} = 1.7\ (K_{CF_3Br})_{min}$$

in both inhibited flames, II and IV. The rates of the reactions occurring between the decay of CF_3Br and the production of HF are not, collectively, very much faster than the CF_3Br decay reactions in this flame.

At the maximum rate of production of HF, z = 0.62 cm and T = 1,720 K, the observed K_{HF} is 10.2×10^{-6} mole cm^{-3} sec^{-1}. A production rate for HF at this point in the flame can be calculated by assigning to the reactions listed earlier the upper limit rate coefficient determined from the analyses of other species involved in the reaction; for example, from the K_{CF_2} analysis for reaction 23. For reactions 31 and 32, the rate coefficient[2] was assumed to be that of the analogous CH_3 reaction, although for reaction 32 a factor of 10 increase in the rate coefficient made no difference in the conclusion. The assumption was made that all of the reactions listed giving HF or F resulted in the maximum possible rate of HF production so that, for example, reaction 27a yielded a contribution to K_{HF} equal to twice the rate calculated for the rate of the reaction of CF_2+O. Each F atom produced is assumed to rapidly react to give HF. The maximum rate of HF production calculated in this manner was 13.3×10^{-6} mole cm^{-3} sec^{-1}. This value represents quite reasonable agreement with the observed K_{HF}(max), 10.2×10^{-6} mole cm^{-3} sec^{-1}, in view of the uncertainties in the rate data. Without the assumption of maximum HF production rate from each reaction or the use of lower limit rate coefficients, a calculated K_{HF} that is 2 to 2.5 times, respectively, lower than the observed K_{HF} is obtained.

From this type of calculation at various points in the flame, we identify the most important reactions for HF production. We find that for z < 0.5 cm, the low z foot of the K_{HF} profile is accounted for by the reactions (in order of importance)

$$CF_3 + H \rightarrow CF_2 + HF$$

$$CF_2 + H \rightarrow CF + HF$$

$$CF_2 + OH \rightarrow CO + HF + F$$

Near the maximum rate of production of HF, the reaction of CF_2+O joins these three reactions as a major contributor to HF production, but it does not dominate. Thus, although the net reaction rate profiles for both F_2CO and HF show an unusual low z foot and both begin to increase rapidly where the concentration of oxygen atoms in the flame begins to increase rapidly, the correlation is significant for F_2CO but not for HF.

Br_2.--Molecular bromine was not observed in the flame containing 0.3% CF_3Br initially (7). Analysis of the formation rate of CH_3Br at low temperature in that flame suggested that molecular bromine must occur in the flame at low values of z. Thus, the observation of Br_2 in the present flame was expected, and its maximum at very low z values provided gratifying confirmation of the earlier analysis. The maximum mole fraction observed for Br_2 is 2.6×10^{-5}, and this may be in error by an order of magnitude because of the uncertainties in the cross sections used to estimate the concentration of Br_2 relative to that of CF_3Br. The uncertainty in the net reaction rate for Br_2 will be about the same as the uncertainty in the mole fraction.

In spite of the large range of uncertainty we cannot account for the observed rate of formation of Br_2 in this flame. The reactions that may reasonably be expected to produce Br_2 in the flame are

$$Br + CF_3Br \rightarrow Br_2 + CF_3 \quad (33)$$

$$Br + CH_3Br \rightarrow Br_2 + CH_3 \quad (34)$$

$$Br + HBr \rightarrow Br_2 + H \quad (35)$$

$$Br + Br + M \rightarrow Br_2 + M \quad (36)$$

Assuming that the reverse reactions are not important, which provides for a maximum possible production rate for Br_2, we calculate a total net reaction rate for Br_2 at 850 K of $\sim 10^{-10}$ mole cm^{-3} sec^{-1}. This is more than two orders of magnitude lower than the observed maximum net reaction rate for Br_2. The rate coefficients used in these calculations were 8.13×10^{13} exp(-25,170/RT) for reaction 33 (20), 5×10^{13} exp(-22,900/RT) for reaction 34 (32), and 2.7×10^{14} exp(-22,200/T) for reaction 35 (18). For reaction 36 the rate coefficient was calculated from the recommended recombination rate coefficient for Ar as a third body, M: $\log k_{36\text{-Ar}} = 15.381 - 2.287 \log(T/300) + 1.154 \log^2(T/300)$ (14).

A possible additional source of Br_2 is recombination of Br at the burner surface. If this were the primary source of molecular bromine we would expect to observe a concentration profile for Br_2 having the appearance of reactant profiles with the maximum concentration at the burner surface. The net reaction rate profile would also have its maximum at the burner surface in that case. The concentration of Br_2 as close to the burner surface as we can reliably sample is about 1/3 of the maximum; surface recombination undoubtedly occurs, but it does not appear to be the principal source of Br_2.

Two modeling studies of H_2/O_2 flames inhibited with HBr predict molecular bromine with a concentration maximum occurring close to the cold gas boundary (18, 23). Galant attributes the Br_2 behavior to reaction 36 and the reverse of reaction 35 in the H_2/O_2 flame. From our observations either a Br_2-producing reaction different from reactions 33-36 is important in methane flames, or the recombination of Br atoms in these flames is, for reasons not known, anomalously fast.

SUMMARY

The microstructure, including radical species, of nearly stoichiometric CH_4-O_2-Ar flames containing initially 1.1% CF_3Br has been determined. These data are analyzed in light of previous microstructure studies of flames containing 0.3% CF_3Br initially and of the analogous clean flame.

Comparison of the maximum concentration of inhibitor-related species in flames initially containing 1.1% and 0.3% CF_3Br suggests that similar mechanisms for formation and decay of these species are operating in both flames. These reactions, as well as those responsible for the disappearance of the major reactants and production of the major products, are shifted to higher temperatures in the presence of 1.1% CF_3Br. The effects of this inhibitor on the net reaction rate curves for methane and oxygen, and on the maximum concentration of formaldehyde, are similar to effects observed with HBr in very lean flames where different chain carriers predominate in the preheat zone of the flame.

The different temperature regions for the primary reaction zones in the inhibited versus the analogous clean flame account for the greater maximum CH_3 concentration in the former. The difference in formaldehyde maxima between the inhibited and clean flames is consistent with a mechanism of decay for that species that includes a large contribution from thermal decomposition reactions.

The behavior of CF_3Br in the 1.1% flame is different from its behavior in the 0.3% flame. Its net reaction rate both is shifted to higher temperature and is narrower in the flame containing more inhibitor. By analogy to the major reactants, we conclude that the decay of CF_3Br is also delayed on account of the reduction of radicals at low temperature in the inhibited relative to the clean flame. This observation is inconsistent with the idea of a zone of inhibition just prior to the primary reaction zone in which the inhibitor and/or its decomposition products scavenge radicals in direct competition with chain-branching reactions.

Analysis of the decay of CF_3Br suggests that, in contrast to the earlier study, the inhibitor is consumed not only by reaction with H, but also by thermal decomposition. Each pathway is equally important at the maximum rate of decay of CF_3Br.

From analyses of the net reaction rate profiles of the bromine- and fluorine-containing species observed, mechanisms to account for the formation of these species in the primary reaction zone of the flame have been deduced. The observation of the CF_2 radical and of CF_3H, from which a profile for the CF_3 radical may be calculated, provided critically important information. The presence of molecular bromine, though anticipated, cannot be accounted for quantitatively. The reactions judged to be primarily responsible for the major stable species containing fluorine are collected in table 4. They are, for the most part, radical-radical reactions involving CF_2, and the fluorocarbon chemistry occurring in this flame is due primarily to the CF_2 and not the CF_3 radical, as originally postulated (7). Rate coefficients for these

and the reactions of other species related to the presence of the inhibitor were determined, and the results are given in table 5.

TABLE 4. - Reactions responsible for the formation of fluorocarbons in CF_3Br-inhibited flames

CH_2CF_2	$CH_3+CF_2 \rightarrow (CF_2CH_3)^* \rightarrow CH_2CF_2+H$
F_2CO	$CF_2+OH \rightarrow F_2CO+H$
	$CF_2+O \rightarrow F_2CO$
	$CH_2CF_2+O \rightarrow F_2CO+CH_2$
HF	$CF_3+H \rightarrow HF+CF_2$
	$CF_2+H \rightarrow HF+CF$
	$CF_2+OH \rightarrow HF+CO+F$
	$CF_2+O \rightarrow CO+\underbrace{F+F}$
	$+2RH \rightarrow 2HF+2R$

*Denotes a vibrationally excited molecule.

TABLE 5. - Summary of rate coefficients determined from kinetic analysis of a methane-oxygen-argon flame containing 1.1% CF_3Br initially

Reaction	Temperature range, K	k, cm^3 $mole^{-1}$ sec^{-1}
$CH_3+CF_3Br \rightarrow CH_3Br+CF_3$	900-1,600	5.8×10^{12} exp(-4,200/RT)
$CF_3H+M \rightarrow CF_3+H+M$	1,845	2×10^{10}
$CH_3+CF_2 \rightarrow \ldots \rightarrow CF_2CH_2+H$	1,300-1,600	2×10^{13}
$CF_3+H \rightarrow HF+CF_2$	1,800	$\leq 8\times10^{14}$
$CF_2+(H,OH,O) \rightarrow$ product	1,800	3×10^{13}
$CF_2+OH \rightarrow F_2CO+H$	1,090-1,375	5×10^{12}
$CF_2+O \rightarrow F_2CO$	1,495-1,780	$\sim10^{13}$
$CH_2CF_2+O \rightarrow F_2CO+CH_2$		

REFERENCES

1. Barnes, G. R., R. A. Cox, and R. F. Simmons. The Kinetics of the Gas-Phase Thermal Decomposition of Chlorodifluoromethane. J. Chem. Soc. (B), 1971, pp. 1176-1180.

2. Bauer, S. H., K. C. Hou, and E. L. Resler, Jr. Single-Pulse Shock-Tube Studies of the Pyrolysis of Fluorocarbons and of the Oxidation of Perfluoroethylene. Phys. Fluids Supplement I, 1969, pp. I-125-I-132.

3. Benson, S. W., and H. E. O'Neal. Kinetic Data on Gas Phase Unimolecular Reactions. NBS, Stand. Ref. Data Series, No. 21, 1970, p. 501.

4. Biordi, J. C., C. P. Lazzara, and J. F. Papp. Flame Structure Studies of CF_3Br Inhibited Methane Flames. Proc. 14th Internat. Symp. on Combustion, Combustion Institute, Pittsburgh, Pa., 1973, pp. 367-381.

5. _____. Molecular Beam Mass Spectrometry Applied to Determining the Kinetics of Reactions in Flames. I. Empirical Characterization of Flame Perturbation by Molecular Beam Sampling Probes. Combustion and Flame, v. 23, 1974, pp. 73-82.

6. _____. The Rate Coefficient for $H+CH_4 \rightarrow H_2+CH_3$ in the Temperature Range 1300-1700° K. J. Chem. Phys., v. 61, No. 2, 1974, pp. 741-742.

7. _____. Chemical Flame Inhibition Using Molecular Beam Mass Spectrometry. Reaction Rates and Mechanisms in a 0.3 Percent CF_3Br Inhibited Methane Flame. BuMines RI 8029, 1975, 42 pp.

8. _____. Flame Structure Studies of CF_3Br-Inhibited Methane Flames. II. Kinetics and Mechanisms. Proc. 15th Internat. Symp. on Combustion, Combustion Institute, Pittsburgh, Pa., 1975, pp. 917-932.

9. _____. The Effect of CF_3Br on Radical Concentration Profiles in Methane Flames. Ch. in Halogenated Fire Suppressants, ed. by R. G. Gann. ACS Symp. Series No. 16, 1975, pp. 256-294.

10. _____. Molecular Beam Mass Spectrometry Applied to Determining the Kinetics of Reactions in Flames. II. Critique of the Method for Rate Coefficient Determinations. Combustion and Flame, v. 26, 1976, pp. 57-76.

11. _____. Mass Spectrometric Observation of Difluorocarbene and Its Reactions in Inhibited Methane Flames. J. Phys. Chem., v. 80, 1976, pp. 1042-1048.

12. _____. Flame Structure Studies of CF_3Br Inhibited Methane Flames. 3. The Effect of 1% CF_3Br on Composition, Rate Constants, and Net Reaction Rates. J. Phys. Chem., v. 81, 1977, pp. 1139-1145.

13. _____. Flame Structure Studies of CF_3Br Inhibited Methane Flames. IV. Reactions of Inhibitor Related Species in Flames Containing Initially 1.1 Percent CF_3Br. J. Phys. Chem., v. 82, 1978, pp. 125-132.

14. Brown, N. J. Halogen Kinetics Pertinent to Flame Inhibition: A Review. Ch. in Halogenated Fire Suppressants, ed. by R. G. Gann. ACS Symp. Series No. 16, 1975, pp. 341-375.

15. Clark, T. C., and J. E. Dove. Examination of Possible Non-Arrhenius Behavior in the Reactions $H+C_2H_6 \rightarrow H_2+C_2H_5$, $H+CH_4 \rightarrow H_2+CH_3$, $CH_3+C_2H_6 \rightarrow CH_4+C_2H_5$. Can. J. Chem., v. 51, 1973, pp. 2147-2154.

16. Cordiero, A. A., P. M. Becker, and R. J. Heinsohn. Computer Simulations of Two Lean Premixed Methane-Oxygen Flames. Pennsylvania State University, University Park, Pa., 1972, 33 pp.

17. Cox, R. A., and R. F. Simmons. The Kinetics of the Gas-Phase Thermal Decomposition of Bromodifluoromethane. J. Chem. Soc. (B), 1971, pp. 1625-1631.

18. Day, J. J., D. V. Stamp, K. Thompson, and G. Dixon-Lewis. Inhibition of Hydrogen-Air and Hydrogen-Nitrous Oxide Flames by Halogen Compounds. Proc. 13th Internat. Symp. on Combustion, Combustion Institute, Pittsburgh, Pa., 1971, pp. 705-712.

19. Fenimore, C. P. Destruction of Methane in Water Gas by Reaction of CH_3 With OH Radicals. Proc. 12th Internat. Symp. on Combustion, Combustion Institute, Pittsburgh, Pa., 1969, pp. 463-467.

20. Ferguson, K. C., and E. Whittle. Kinetics of the Reaction Between HBr and CF_3Br. J. Chem. Soc., Faraday Trans., v. 68, No. 1, 1972, pp. 295-305.

21. Field, F. H., and J. F. Franklin. Electron Impact and Ionization Phenomena. Academic Press, New York, rev. ed., 1970, pp. 239-493.

22. Fristrom, R. M., and A. A. Westenberg. Flame Structure. McGraw-Hill Book Co., Inc., New York, 1965, 424 pp.

23. Galant, S., and J. P. Appleton. Theoretical Investigation of Inhibition Phenomena in Halogenated Flames. Ch. in Halogenated Fire Suppressants, ed. by R. G. Gann. ACS Symp. Series No. 16, 1975, pp. 406-427.

24. Giles, R. D., and E. Whittle. Photolysis of Mixtures of Acetone and Hexafluoroacetone. Trans. Faraday Soc., v. 61, 1965, pp. 1425-1436.

25. Hsu, D. S. Y., M. E. Umstead, and M. C. Lin. Kinetics and Mechanisms of Reactions of Fluoromethylidyne, Monofluoromethylene, and Difluoromethylene Radicals. In Fluorine-Containing Free Radicals. ACS Symp. Series No. 66, 1978, pp. 128-151.

26. Izod, T. P. J., G. B. Kistiakowsky, and S. Matsuda. Oxidation of Carbon Monoxide Mixtures With Added Ethane or Azomethane Studied in Incident Shock Waves. J. Chem. Phys., v. 55, 1971, pp. 4425-4432.

27. Jones, D. S., and S. J. Moss. Arrhenius Parameters for Reactions of Oxygen Atoms With the Fluorinated Ethylenes. Internat. J. Chem. Kinetics, v. 6, 1974, pp. 443-452.

28. Kaskan, W. E. The Dependence of Flame Temperature on Mass Burning Velocity. Proc. 6th Internat. Symp. on Combustion, Combustion Institute, Pittsburgh, Pa., 1957, pp. 134-143.

29. Kaskan, W. E., and J. J. Reuther. Limiting Equivalence Ratio, Dissociation, and Self-Inhibition in Premixed, Quenched, Fuel-Rich Hydrocarbon/Air Flames. Proc. 16th Internat. Symp. on Combustion, Combustion Institute, Pittsburgh, Pa., 1977, pp. 1083-1095.

30. Keating, E. L., and R. A. Matula. COF_2 Formation: The High Temperature C_2F_4-O_2 Reaction System. Pres. at the 1973 Fall Meeting of the Eastern States Section of the Combustion Institute, McGill University, Montreal, Quebec, Canada, Oct. 11-12, 1973, 18 pp.; available from Combustion Kinetics Lab., Dept. Mech. Eng. and Mechanics, Drexel Univ., Philadelphia, Pa.

31. Kobrinsky, P. C., G. O. Pritchard, and S. Toby. Pressure Dependence of the Cross-Combination Ratio for CF_3 and CH_3 Radicals. J. Phys. Chem., v. 75, 1971, pp. 2225-2226.

32. Kondratiev, V. N. Rate Constants of Gas Phase Reactions (trans. by L. J. Holtschlag and ed. by R. M. Fristrom). NBS, COM-72-10014, 1972, 428 pp.

33. Laufer, A. H., and A. M. Bass. Mechanism and Rate Constant of the Reaction Between Methylene and Methyl Radicals. J. Phys. Chem., v. 79, 1975, pp. 1635-1638.

34. Lazzara, C. P., J. C. Biordi, and J. F. Papp. Concentration Profiles for Radical Species in a Methane-Oxygen-Argon Flame. Combustion and Flame, v. 21, 1973, pp. 371-382.

35. Lifshitz, C., and F. A. Long. Appearance Potentials and Mass Spectra of Fluorinated Ethylenes. I. Decomposition Mechanisms and Their Energetics. J. Phys. Chem., v. 67, 1963, pp. 2463-2468.

36. _____. Appearance Potentials and Mass Spectra of Fluorinated Ethylenes. II. Heats of Formation of Fluorinated Species and Their Positive Ions. J. Phys. Chem., v. 69, 1965, pp. 3731-3736.

37. Mitchell, R. C., and J. P. Simons. The Reaction of $O(2^3P)$ Atoms With 1,1-Difluoro-olefins. J. Chem. Soc. (B), v. 80, 1968, pp. 1005-1007.

38. Mitsch, R. A., and A. S. Rogers. Reactivities in Olefin-Difluorocarbene Reactions. Internat. J. Chem. Kinetics, v. 1, 1969, pp. 439-450.

39. Modica, A. P., and J. E. LaGraff. Decomposition and Oxidation of C_2F_4 Behind Shock Waves. J. Chem. Phys., v. 43, 1965, pp. 3383-3392.

40. Papp, J. F., C. P. Lazzara, and J. C. Biordi. Chemical Flame Inhibition Using Molecular Beam Mass Spectrometry. Computational Methods for Analyzing Flame Microstructure. BuMines RI 8019, 1975, 90 pp.

41. Peeters, J., and G. Mahnen. Reaction Mechanisms and Rate Constants of Elementary Steps in Methane-Oxygen Flames. Proc. 14th Internat. Symp. on Combustion, Combustion Institute, Pittsburgh, Pa., 1973, pp. 133-146.

42. Pilling, M. J., and J. A. Robertson. A Rate Constant for $CH_2(^3B_1)+CH_3$. Chem. Phys. Letters, v. 33, 1975, pp. 336-339.

43. Pritchard, G. O., and M. J. Perona. The Elimination of HF From Vibrationally Excited Fluoroethanes. The Decomposition of 1,1,1-Trifluoroethane-d_0 and d_3. Internat. J. Chem. Kinetics, v. 2, 1970, pp. 281-297.

44. Roth, P., and Th. Just. Atom-Resonanzaborptionsmessungen beim thermischen Zerfall von Methon hinter Stosswellen (Atom Resonance Absorption Measurement of the Thermal Decomposition of Methane Behind a Shock Wave). Ber. Bunsenges. Phys. Chem., v. 79, No. 8, 1975, pp. 682-686.

45. Sehon, A. H., and M. Szwarc. The C-Br Bond Dissociation Energy in Halogenated Bromomethanes. Proc. Royal Soc. London, Ser. A, v. 209, 1951, pp. 110-131.

46. Skinner, G. B. Inhibition of the Hydrogen-Oxygen Reaction by CF_3Br and CF_2BrCF_2Br. Ch. in Halogenated Fire Suppressants, ed. by R. G. Gann. ACS Symp. Series No. 16, 1975, pp. 295-317.

47. Tedder, J. M., and J. C. Walton. Reactions of Halogenomethyl Radicals. Progress in Reaction Kinetics, v. 4, 1967, pp. 37-61.

48. Trotmann-Dickenson, A. F., and G. S. Milne. Tables of Bimolecular Gas Reactions. NBS, NSRDS-NBS 9, 1967, 129 pp.

49. Tschuikow-Roux, E., and J. E. Marte. Thermal Decomposition of Fluoroform in a Single-Pulse Shock Tube. I. J. Chem. Phys., v. 42, 1965, pp. 2049-2056.

50. Vandorren, J., J. Peeters, and P. J. Van Tiggelen. Rate Constants of the Elementary Reaction of Carbon Monoxide With Hydroxyl Radical. Proc. 15th Internat. Symp. on Combustion, Combustion Institute, Pittsburgh, Pa., 1975, pp. 745-753.

51. Westenberg, A. A., and N. deHaas. Measurement of the Rate Constant for $H+H_2CO \rightarrow H_2+HCO$ at 297-652° K. J. Phys. Chem., v. 76, No. 16, 1972, pp. 2213-2214.

52. Wilson, W. E., J. T. O'Donovan, and R. M. Fristrom. Flame Inhibition by Halogen Compounds. Proc. 12th Internat. Symp. on Combustion, Combustion Institute, Pittsburgh, Pa., 1969, pp. 929-942.

53. Wise, H., and W. A. Rosser. Homogeneous and Heterogeneous Reactions of Flame Intermediates. Proc. 9th Internat. Symp. on Combustion, Combustion Institute, Pittsburgh, Pa., 1963, pp. 733-746.

APPENDIX A.--FLAME SPECIES SMOOTHED COMPOSITION PROFILES

This appendix contains a partial listing (every fifth value) of the smoothed species composition profiles determined for the uninhibited flame III and the inhibited flame IV containing 1.1% CF_3Br. The characteristics of both flames are given in table A-1.

TABLE A-1. - Characteristics of flames III and IV examined at 0.042 atm

	Flame III	Flame IV
Flow, g sec^{-1}:		
CH_4	0.0107	0.0108
O_2	0.0456	0.0455
Ar	0.1811	0.1808
CF_3Br	0	0.0110
CH_4, mole-pct	10.1	10.1
O_2, mole-pct	21.5	21.2
Ar, mole-pct	68.4	67.6
CF_3Br, mole-pct	0	1.1
V_o[1], cm sec^{-1}	47.6	48.0
T_{max}[2], K	1,781	1,966
T_{ad}[3], K	2,375	2,358

[1] Cold gas velocity calculated using $T_{initial}$ = 298 K.

[2] As determined in the absence of the sampling probe (5).

[3] Calculated adiabatic flame temperature.

These smoothed mole fraction profiles are obtained by applying various smoothing techniques to the mole fractions calculated from mass spectral intensities and calibration factors (7, 40).[1] The numbers under the column heading INDEX (tables A-2-A-4) are used in the computer program to identify each position. The numbers under the column heading Z are the distances, in centimeters, between the sampling probe tip and the burner surface. (Z = 0.0 is the burner surface.) The numbers in the column labeled TEMP are the smoothed temperature profiles in kelvins. The temperature profiles have been shifted to account for the probe "cooling" effect as described in reference 5. The temperatures given are those used in the kinetic analyses of the flames. The remaining columns are the mole fractions of the species listed at the head of the column. These smoothed mole fraction profiles appear as solid lines plotted through the data points in figures 2-7 of the text. The smoothed temperature profiles appear as the dashed line in the figures. The argon (column labeled A) mole fraction varies through the flame because it is defined to be the difference between 1 and the sum of all the other species mole fractions, $X_{Ar} = 1 - \sum_i X_i$, where $i \neq Ar$.

[1] Underlined numbers in parentheses refer to items in the list of references preceding the appendixes.

TABLE A-2. - Smoothed composition profiles for the species in flame III

			MOLE FRACTION											
INDEX	Z	TEMP	CH4	CO	CO2	H	H2O	OH	A	H2	O2	O	H2CO	CH3
5	.020	300.	.805E-01	.636E-02	.230E-02	0.	.207E-01	0.	.678E+00	.119E-01	.200E+00	0.	.170E-03	.940E-05
10	.045	300.	.791E-01	.732E-02	.267E-02	0.	.231E-01	0.	.677E+00	.125E-01	.198E+00	0.	.230E-03	.218E-04
15	.070	349.	.770E-01	.868E-02	.325E-02	.208E-04	.266E-01	.170E-04	.676E+00	.132E-01	.195E+00	0.	.293E-03	.356E-04
20	.095	418.	.742E-01	.104E-01	.403E-02	.764E-04	.310E-01	.615E-04	.676E+00	.140E-01	.190E+00	0.	.353E-03	.526E-04
25	.120	496.	.710E-01	.124E-01	.499E-02	.157E-03	.360E-01	.125E-03	.675E+00	.149E-01	.185E+00	0.	.407E-03	.804E-04
30	.145	579.	.676E-01	.147E-01	.612E-02	.253E-03	.415E-01	.197E-03	.674E+00	.158E-01	.179E+00	0.	.469E-03	.129E-03
35	.170	667.	.639E-01	.170E-01	.739E-02	.361E-03	.473E-01	.271E-03	.673E+00	.167E-01	.173E+00	0.	.539E-03	.198E-03
40	.195	758.	.602E-01	.195E-01	.881E-02	.487E-03	.533E-01	.344E-03	.672E+00	.177E-01	.167E+00	0.	.592E-03	.282E-03
45	.220	852.	.564E-01	.222E-01	.104E-01	.643E-03	.595E-01	.415E-03	.671E+00	.186E-01	.160E+00	0.	.627E-03	.378E-03
50	.245	946.	.525E-01	.250E-01	.120E-01	.844E-03	.658E-01	.484E-03	.669E+00	.196E-01	.154E+00	0.	.666E-03	.490E-03
55	.270	1037.	.484E-01	.280E-01	.139E-01	.110E-02	.722E-01	.554E-03	.668E+00	.205E-01	.146E+00	.149E-04	.716E-03	.631E-03
60	.295	1122.	.442E-01	.310E-01	.158E-01	.140E-02	.790E-01	.632E-03	.666E+00	.214E-01	.139E+00	.447E-04	.766E-03	.807E-03
65	.320	1200.	.397E-01	.340E-01	.179E-01	.175E-02	.862E-01	.731E-03	.665E+00	.224E-01	.130E+00	.935E-04	.812E-03	.101E-02
70	.345	1270.	.350E-01	.370E-01	.201E-01	.216E-02	.936E-01	.868E-03	.664E+00	.232E-01	.121E+00	.171E-03	.855E-03	.124E-02
75	.370	1333.	.302E-01	.398E-01	.224E-01	.262E-02	.101E+00	.106E-02	.663E+00	.240E-01	.113E+00	.294E-03	.883E-03	.145E-02
80	.395	1391.	.256E-01	.424E-01	.249E-01	.315E-02	.109E+00	.134E-02	.662E+00	.246E-01	.104E+00	.480E-03	.883E-03	.162E-02
85	.420	1442.	.211E-01	.446E-01	.274E-01	.378E-02	.116E+00	.171E-02	.660E+00	.250E-01	.964E-01	.744E-03	.851E-03	.170E-02
90	.445	1488.	.170E-01	.465E-01	.302E-01	.450E-02	.123E+00	.219E-02	.658E+00	.252E-01	.892E-01	.109E-02	.793E-03	.166E-02
95	.470	1526.	.134E-01	.480E-01	.330E-01	.531E-02	.130E+00	.278E-02	.655E+00	.252E-01	.828E-01	.153E-02	.710E-03	.151E-02
100	.495	1559.	.101E-01	.493E-01	.360E-01	.617E-02	.137E+00	.345E-02	.652E+00	.249E-01	.771E-01	.206E-02	.609E-03	.129E-02
105	.520	1586.	.744E-02	.501E-01	.390E-01	.704E-02	.143E+00	.420E-02	.649E+00	.243E-01	.721E-01	.268E-02	.496E-03	.103E-02
110	.545	1608.	.526E-02	.506E-01	.419E-01	.790E-02	.148E+00	.500E-02	.646E+00	.236E-01	.676E-01	.337E-02	.381E-03	.763E-03
115	.570	1627.	.358E-02	.505E-01	.447E-01	.872E-02	.153E+00	.580E-02	.643E+00	.227E-01	.634E-01	.411E-02	.275E-03	.534E-03
120	.595	1642.	.236E-02	.499E-01	.472E-01	.949E-02	.156E+00	.659E-02	.641E+00	.217E-01	.597E-01	.487E-02	.190E-03	.358E-03
125	.620	1654.	.151E-02	.488E-01	.496E-01	.102E-01	.159E+00	.733E-02	.641E+00	.207E-01	.563E-01	.561E-02	.127E-03	.227E-03
130	.645	1662.	.961E-03	.473E-01	.518E-01	.109E-01	.161E+00	.798E-02	.640E+00	.198E-01	.532E-01	.628E-02	.798E-04	.141E-03
135	.670	1667.	.616E-03	.455E-01	.539E-01	.114E-01	.163E+00	.854E-02	.641E+00	.190E-01	.506E-01	.685E-02	.450E-04	.934E-04
140	.695	1671.	.408E-03	.436E-01	.559E-01	.120E-01	.164E+00	.899E-02	.641E+00	.183E-01	.483E-01	.730E-02	.231E-04	.672E-04
145	.720	1674.	.279E-03	.417E-01	.580E-01	.124E-01	.165E+00	.934E-02	.641E+00	.176E-01	.465E-01	.763E-02	.124E-04	.475E-04
150	.745	1677.	.192E-03	.398E-01	.601E-01	.128E-01	.166E+00	.960E-02	.642E+00	.171E-01	.451E-01	.788E-02	.804E-05	.317E-04
155	.770	1679.	.123E-03	.380E-01	.621E-01	.132E-01	.166E+00	.980E-02	.642E+00	.167E-01	.440E-01	.805E-02	.560E-05	.215E-04
160	.795	1681.	.639E-04	.364E-01	.640E-01	.136E-01	.166E+00	.995E-02	.642E+00	.163E-01	.432E-01	.819E-02	.353E-05	.168E-04
165	.820	1681.	.202E-04	.349E-01	.657E-01	.140E-01	.167E+00	.101E-01	.642E+00	.160E-01	.425E-01	.829E-02	.194E-05	.149E-04
170	.845	1681.	0.	.335E-01	.672E-01	.144E-01	.167E+00	.102E-01	.642E+00	.158E-01	.418E-01	.836E-02	.755E-06	.132E-04
175	.870	1681.	0.	.323E-01	.685E-01	.147E-01	.167E+00	.103E-01	.642E+00	.156E-01	.410E-01	.841E-02	0.	.111E-04
180	.895	1680.	0.	.311E-01	.696E-01	.149E-01	.168E+00	.103E-01	.643E+00	.155E-01	.400E-01	.845E-02	0.	.894E-05
185	.920	1679.	0.	.301E-01	.706E-01	.151E-01	.168E+00	.104E-01	.643E+00	.154E-01	.390E-01	.849E-02	0.	.682E-05
190	.945	1678.	0.	.292E-01	.715E-01	.151E-01	.168E+00	.105E-01	.644E+00	.153E-01	.382E-01	.852E-02	0.	.463E-05
195	.970	1676.	0.	.284E-01	.724E-01	.152E-01	.168E+00	.105E-01	.644E+00	.152E-01	.377E-01	.856E-02	0.	.235E-05
200	.995	1674.	0.	.276E-01	.734E-01	.152E-01	.168E+00	.106E-01	.644E+00	.152E-01	.375E-01	.861E-02	0.	.459E-06

TABLE A-3. - Smoothed composition profiles for the species unrelated to the inhibitor in flame IV

			MOLE FRACTION											
INDEX	Z	TEMP	CH4	CO	CO2	H	H2O	OH	A	H2	O2	O	H2CO	CH3
5	.020	300.	.854E-01	.156E-02	.324E-03	.129E-05	.503E-02	0.	.684E+00	.829E-02	.203E+00	0.	0.	.345E-05
10	.045	300.	.855E-01	.211E-02	.616E-03	.286E-05	.634E-02	0.	.679E+00	.883E-02	.205E+00	0.	0.	.776E-05
15	.070	300.	.854E-01	.273E-02	.889E-03	.425E-05	.783E-02	0.	.675E+00	.942E-02	.206E+00	0.	.523E-06	.121E-04
20	.095	300.	.847E-01	.343E-02	.117E-02	.515E-05	.954E-02	0.	.672E+00	.100E-01	.205E+00	0.	.362E-05	.164E-04
25	.120	349.	.835E-01	.423E-02	.147E-02	.539E-05	.115E-01	0.	.671E+00	.107E-01	.204E+00	0.	.735E-05	.207E-04
30	.145	427.	.820E-01	.513E-02	.184E-02	.530E-05	.136E-01	0.	.670E+00	.113E-01	.201E+00	0.	.121E-04	.250E-04
35	.170	510.	.802E-01	.613E-02	.227E-02	.609E-05	.158E-01	0.	.670E+00	.120E-01	.198E+00	0.	.174E-04	.293E-04
40	.195	597.	.783E-01	.724E-02	.278E-02	.979E-05	.182E-01	.293E-05	.670E+00	.127E-01	.195E+00	0.	.226E-04	.336E-04
45	.220	684.	.762E-01	.841E-02	.337E-02	.187E-04	.207E-01	.146E-04	.670E+00	.134E-01	.191E+00	0.	.279E-04	.380E-04
50	.245	769.	.740E-01	.976E-02	.406E-02	.344E-04	.235E-01	.361E-04	.669E+00	.141E-01	.187E+00	0.	.331E-04	.423E-04
55	.270	853.	.714E-01	.113E-01	.487E-02	.575E-04	.268E-01	.665E-04	.669E+00	.148E-01	.182E+00	0.	.383E-04	.463E-04
60	.295	934.	.685E-01	.130E-01	.585E-02	.871E-04	.306E-01	.103E-03	.667E+00	.156E-01	.178E+00	0.	.434E-04	.499E-04
65	.320	1014.	.654E-01	.150E-01	.704E-02	.122E-03	.351E-01	.139E-03	.666E+00	.163E-01	.173E+00	0.	.484E-04	.544E-04
70	.345	1090.	.622E-01	.172E-01	.843E-02	.163E-03	.400E-01	.172E-03	.663E+00	.170E-01	.168E+00	0.	.533E-04	.661E-04
75	.370	1165.	.588E-01	.197E-01	.100E-01	.212E-03	.453E-01	.197E-03	.660E+00	.177E-01	.162E+00	0.	.584E-04	.105E-03
80	.395	1238.	.553E-01	.223E-01	.118E-01	.273E-03	.507E-01	.214E-03	.657E+00	.185E-01	.156E+00	0.	.643E-04	.192E-03
85	.420	1307.	.516E-01	.250E-01	.136E-01	.348E-03	.561E-01	.226E-03	.654E+00	.193E-01	.150E+00	0.	.735E-04	.317E-03
90	.445	1374.	.477E-01	.279E-01	.155E-01	.439E-03	.615E-01	.235E-03	.652E+00	.201E-01	.144E+00	0.	.860E-04	.456E-03
95	.470	1436.	.435E-01	.310E-01	.175E-01	.544E-03	.671E-01	.248E-03	.650E+00	.210E-01	.137E+00	.350E-04	.992E-04	.636E-03
100	.495	1495.	.390E-01	.343E-01	.197E-01	.666E-03	.731E-01	.279E-03	.648E+00	.219E-01	.129E+00	.102E-03	.112E-03	.912E-03
105	.520	1549.	.342E-01	.379E-01	.220E-01	.819E-03	.798E-01	.350E-03	.646E+00	.228E-01	.121E+00	.202E-03	.127E-03	.128E-02
110	.545	1598.	.293E-01	.416E-01	.246E-01	.104E-02	.872E-01	.492E-03	.643E+00	.235E-01	.113E+00	.329E-03	.147E-03	.170E-02
115	.570	1643.	.244E-01	.450E-01	.275E-01	.139E-02	.951E-01	.746E-03	.640E+00	.240E-01	.104E+00	.477E-03	.171E-03	.208E-02
120	.595	1684.	.196E-01	.481E-01	.307E-01	.192E-02	.103E+00	.115E-02	.637E+00	.242E-01	.945E-01	.662E-03	.195E-03	.232E-02
125	.620	1720.	.151E-01	.507E-01	.340E-01	.266E-02	.111E+00	.175E-02	.635E+00	.241E-01	.856E-01	.930E-03	.220E-03	.233E-02
130	.645	1751.	.111E-01	.525E-01	.374E-01	.361E-02	.119E+00	.258E-02	.632E+00	.237E-01	.772E-01	.135E-02	.223E-03	.206E-02
135	.670	1779.	.762E-02	.536E-01	.408E-01	.471E-02	.126E+00	.362E-02	.630E+00	.230E-01	.697E-01	.197E-02	.196E-03	.160E-02
140	.695	1802.	.493E-02	.539E-01	.443E-01	.585E-02	.133E+00	.486E-02	.626E+00	.220E-01	.633E-01	.280E-02	.163E-03	.112E-02
145	.720	1821.	.299E-02	.535E-01	.477E-01	.695E-02	.138E+00	.621E-02	.623E+00	.210E-01	.580E-01	.379E-02	.132E-03	.727E-03
150	.745	1835.	.173E-02	.524E-01	.512E-01	.794E-02	.143E+00	.757E-02	.619E+00	.198E-01	.537E-01	.485E-02	.993E-04	.445E-03
155	.770	1847.	.976E-03	.509E-01	.546E-01	.879E-02	.147E+00	.881E-02	.615E+00	.187E-01	.501E-01	.585E-02	.617E-04	.265E-03
160	.795	1855.	.559E-03	.491E-01	.577E-01	.954E-02	.150E+00	.983E-02	.613E+00	.177E-01	.472E-01	.671E-02	.272E-04	.164E-03
165	.820	1860.	.328E-03	.471E-01	.604E-01	.102E-01	.152E+00	.106E-01	.612E+00	.168E-01	.447E-01	.738E-02	.445E-05	.106E-03
170	.845	1863.	.189E-03	.451E-01	.627E-01	.107E-01	.153E+00	.110E-01	.612E+00	.160E-01	.426E-01	.787E-02	0.	.618E-04
175	.870	1865.	.967E-04	.432E-01	.646E-01	.112E-01	.154E+00	.113E-01	.613E+00	.154E-01	.408E-01	.821E-02	0.	.239E-04
180	.895	1866.	.361E-04	.414E-01	.662E-01	.116E-01	.153E+00	.115E-01	.615E+00	.149E-01	.394E-01	.844E-02	0.	0.
185	.920	1866.	0.	.398E-01	.679E-01	.118E-01	.153E+00	.116E-01	.616E+00	.144E-01	.382E-01	.860E-02	0.	0.
190	.945	1866.	0.	.384E-01	.695E-01	.120E-01	.153E+00	.117E-01	.617E+00	.141E-01	.372E-01	.872E-02	0.	0.
195	.970	1865.	0.	.373E-01	.712E-01	.122E-01	.153E+00	.118E-01	.617E+00	.138E-01	.364E-01	.882E-02	0.	0.
200	.995	1864.	0.	.363E-01	.727E-01	.123E-01	.153E+00	.119E-01	.617E+00	.136E-01	.357E-01	.890E-02	0.	0.

TABLE A-4. - Smoothed composition profiles for the species related to the inhibitor in flame IV

INDEX	Z	TEMP	MOLE FRACTION											
			CF3BR	HF	HBR	BR	CH3BR	HCO	F2CO	CH2CF2	HO2	BR2	CF3H	CF2
5	.020	300.	.109E-01	.144E-02	.317E-04	0.	.797E-05	0.	.224E-04	.432E-04	0.	.915E-05	.191E-06	0.
10	.045	300.	.109E-01	.176E-02	.465E-04	0.	.938E-05	0.	.320E-04	.553E-04	0.	.106E-04	.677E-06	0.
15	.070	300.	.109E-01	.212E-02	.641E-04	0.	.115E-04	0.	.422E-04	.595E-04	0.	.122E-04	.139E-05	.241E-05
20	.095	300.	.109E-01	.253E-02	.870E-04	0.	.154E-04	0.	.546E-04	.627E-04	0.	.139E-04	.220E-05	.810E-05
25	.120	349.	.109E-01	.299E-02	.115E-03	0.	.211E-04	0.	.711E-04	.691E-04	0.	.157E-04	.319E-05	.155E-04
30	.145	427.	.109E-01	.351E-02	.150E-03	0.	.278E-04	0.	.934E-04	.825E-04	0.	.177E-04	.457E-05	.233E-04
35	.170	510.	.109E-01	.408E-02	.195E-03	0.	.353E-04	0.	.123E-03	.103E-03	0.	.199E-04	.629E-05	.314E-04
40	.195	597.	.109E-01	.471E-02	.253E-03	.284E-04	.443E-04	0.	.161E-03	.127E-03	0.	.221E-04	.791E-05	.403E-04
45	.220	684.	.109E-01	.540E-02	.324E-03	.107E-03	.558E-04	0.	.207E-03	.154E-03	0.	.241E-04	.928E-05	.514E-04
50	.245	769.	.110E-01	.614E-02	.400E-03	.250E-03	.707E-04	0.	.262E-03	.189E-03	0.	.257E-04	.110E-04	.657E-04
55	.270	853.	.110E-01	.694E-02	.476E-03	.466E-03	.890E-04	0.	.324E-03	.235E-03	0.	.262E-04	.137E-04	.843E-04
60	.295	934.	.110E-01	.781E-02	.557E-03	.760E-03	.110E-03	0.	.394E-03	.294E-03	0.	.249E-04	.176E-04	.108E-03
65	.320	1014.	.108E-01	.877E-02	.649E-03	.114E-02	.133E-03	0.	.470E-03	.367E-03	0.	.218E-04	.219E-04	.137E-03
70	.345	1090.	.105E-01	.979E-02	.760E-03	.160E-02	.158E-03	0.	.552E-03	.450E-03	0.	.179E-04	.260E-04	.173E-03
75	.370	1165.	.101E-01	.109E-01	.881E-03	.215E-02	.181E-03	0.	.639E-03	.534E-03	0.	.143E-04	.307E-04	.215E-03
80	.395	1238.	.946E-02	.120E-01	.996E-03	.278E-02	.202E-03	0.	.732E-03	.615E-03	0.	.114E-04	.368E-04	.262E-03
85	.420	1307.	.866E-02	.132E-01	.110E-02	.349E-02	.216E-03	0.	.832E-03	.704E-03	0.	.901E-05	.435E-04	.312E-03
90	.445	1374.	.772E-02	.144E-01	.119E-02	.425E-02	.222E-03	0.	.938E-03	.806E-03	0.	.701E-05	.493E-04	.361E-03
95	.470	1436.	.665E-02	.156E-01	.127E-02	.504E-02	.219E-03	0.	.105E-02	.903E-03	0.	.533E-05	.545E-04	.401E-03
100	.495	1495.	.551E-02	.169E-01	.134E-02	.583E-02	.204E-03	0.	.118E-02	.970E-03	0.	.404E-05	.601E-04	.425E-03
105	.520	1549.	.433E-02	.182E-01	.139E-02	.661E-02	.176E-03	0.	.130E-02	.997E-03	0.	.323E-05	.645E-04	.426E-03
110	.545	1598.	.321E-02	.194E-01	.139E-02	.734E-02	.139E-03	0.	.143E-02	.971E-03	0.	.273E-05	.662E-04	.401E-03
115	.570	1643.	.221E-02	.207E-01	.134E-02	.801E-02	.988E-04	0.	.154E-02	.865E-03	0.	.229E-05	.653E-04	.352E-03
120	.595	1684.	.140E-02	.217E-01	.124E-02	.863E-02	.647E-04	0.	.164E-02	.691E-03	0.	.183E-05	.622E-04	.287E-03
125	.620	1720.	.801E-03	.227E-01	.109E-02	.919E-02	.411E-04	0.	.172E-02	.506E-03	0.	.142E-05	.572E-04	.214E-03
130	.645	1751.	.412E-03	.234E-01	.893E-03	.969E-02	.266E-04	0.	.178E-02	.347E-03	0.	.107E-05	.505E-04	.146E-03
135	.670	1779.	.186E-03	.240E-01	.681E-03	.101E-01	.171E-04	0.	.181E-02	.222E-03	0.	.754E-06	.429E-04	.904E-04
140	.695	1802.	.703E-04	.244E-01	.495E-03	.105E-01	.104E-04	0.	.182E-02	.133E-03	0.	.468E-06	.354E-04	.505E-04
145	.720	1821.	.192E-04	.247E-01	.358E-03	.108E-01	.703E-05	0.	.181E-02	.728E-04	0.	.219E-06	.286E-04	.258E-04
150	.745	1835.	.152E-05	.248E-01	.266E-03	.110E-01	.603E-05	0.	.178E-02	.311E-04	0.	.404E-07	.227E-04	.126E-04
155	.770	1847.	0.	.250E-01	.206E-03	.111E-01	.509E-05	0.	.174E-02	.713E-05	0.	0.	.180E-04	.639E-05
160	.795	1855.	0.	.251E-01	.165E-03	.112E-01	.302E-05	0.	.168E-02	0.	0.	0.	.143E-04	.357E-05
165	.820	1860.	0.	.252E-01	.138E-03	.112E-01	.728E-06	0.	.163E-02	0.	0.	0.	.111E-04	.205E-05
170	.845	1863.	0.	.253E-01	.119E-03	.112E-01	0.	0.	.157E-02	0.	0.	0.	.794E-05	.103E-05
175	.870	1865.	0.	.255E-01	.108E-03	.112E-01	0.	0.	.151E-02	0.	0.	0.	.482E-05	.359E-06
180	.895	1866.	0.	.256E-01	.101E-03	.112E-01	0.	0.	.146E-02	0.	0.	0.	.243E-05	0.
185	.920	1866.	0.	.257E-01	.964E-04	.112E-01	0.	0.	.141E-02	0.	0.	0.	.105E-05	0.
190	.945	1866.	0.	.258E-01	.941E-04	.112E-01	0.	0.	.137E-02	0.	0.	0.	.308E-06	0.
195	.970	1865.	0.	.260E-01	.921E-04	.112E-01	0.	0.	.133E-02	0.	0.	0.	0.	0.
200	.995	1864.	0.	.260E-01	.898E-04	.112E-01	0.	0.	.129E-02	0.	0.	0.	0.	0.

APPENDIX B.--FLAME SPECIES NET REACTION RATE PROFILES

This appendix contains a partial listing (every fifth value) of the net reaction rate profiles determined for the species observed in the uninhibited flame III and the inhibited flame IV containing 1.1% CF_3Br. These net reaction rates were computed according to equations A and B. A description of the physical model for these computations, the method of computation, and a detailed listing of the computer program can be found in reference 40. The numbers under the column heading INDEX are used in the computer program to identify each position. The Z column numbers are the distances, in centimeters, between the sampling probe tip and the burner surface. The TEMP column numbers are a smoothed temperature profile, in kelvins, which has been shifted to account for the probe cooling effect (5).[1] The remaining columns list the net reaction rates, in units of mole cm^{-3} sec^{-1}, for the species at the head of the column. The values of the net reaction rates listed under the argon column, A, are meaningless. These individual net reaction rates, K_i, are the starting point for the kinetic analyses of the flame.

The net reaction rate profiles are very sensitive to small local variations in the smoothed mole fraction profiles. While the order of magnitude and the global variation of the net reaction rates are an accurate representation of the flame system chemistry, the local variations (bumps, glitches, and shoulders) which appear in these rate profiles result from deviations in the smoothed mole fraction profiles. When considered necessary, an effort has been made to minimize local variations in the net reaction rates in the region of the flame where they are used to compute reaction rate coefficients or deduce mechanisms. Figures 8 and 9 in the text are plots of the reaction rate profiles of the species indicated as obtained from this compilation. Certain regions, for example, where the net reaction rate for CH_4 is positive close to the burner, are not shown in the figures. Figures 11, 13, 15, 16, and 17 in the text are plots based on these net reaction rates with local variations removed. The flame region or temperature range over which a particular reaction rate profile can be utilized is limited by the experimental data and the curve-smoothing operation (5).

[1] Underlined numbers in parentheses refer to items in the list of references preceding the appendixes.

TABLE B-1. - Net reaction rate profiles for the species in flame III

			NET REACTION RATE										
INDEX	Z	TEMP	CH4	CO	CO2	H	H2O	OH	A	H2	O2	O	H2CO	CH3
5	.070	349.	.221E-04	-.241E-05	-.167E-05	-.310E-05	-.126E-04	-.433E-06	.659E-06	.462E-05	.211E-04	0.	.136E-06	-.470E-07
10	.095	418.	.128E-04	-.235E-05	-.190E-05	-.251E-05	-.106E-04	-.293E-06	.166E-05	-.181E-05	.134E-04	0.	.109E-06	-.193E-06
15	.120	496.	.851E-05	-.137E-05	-.205E-05	-.216E-05	-.714E-05	-.164E-06	.414E-05	-.210E-05	.820E-05	0.	-.191E-07	-.366E-06
20	.145	579.	.484E-05	-.166E-06	-.219E-05	-.215E-05	-.370E-05	-.199E-07	.650E-05	-.251E-05	.282E-05	0.	.444E-07	-.401E-06
25	.170	667.	.215E-05	-.159E-05	-.235E-05	-.320E-05	-.847E-06	.746E-07	.942E-05	-.311E-05	-.592E-06	0.	.340E-06	-.302E-06
30	.195	758.	.602E-06	-.102E-05	-.255E-05	-.536E-05	.517E-06	.111E-06	.783E-05	-.363E-05	-.606E-06	0.	.345E-06	-.266E-06
35	.220	852.	.509E-06	-.307E-06	-.263E-05	-.800E-05	-.779E-06	.846E-07	.388E-05	-.501E-05	.228E-05	-.105E-06	-.257E-08	-.444E-06
40	.245	946.	.767E-06	-.747E-06	-.261E-05	-.102E-04	-.430E-05	-.433E-07	.486E-06	-.638E-05	.665E-05	-.550E-06	-.129E-06	-.787E-06
45	.270	1037.	.115E-05	.100E-05	-.239E-05	-.112E-04	-.866E-05	-.342E-06	-.330E-05	-.709E-05	.889E-05	-.750E-06	.485E-07	-.101E-05
50	.295	1122.	.724E-06	.367E-05	-.198E-05	-.115E-04	-.108E-04	-.886E-06	-.398E-05	-.564E-05	.638E-05	-.944E-06	.152E-06	-.834E-06
55	.320	1200.	-.179E-05	.641E-05	-.144E-05	-.122E-04	-.801E-05	-.169E-05	-.530E-06	-.687E-06	-.158E-05	-.151E-05	.224E-06	-.197E-06
60	.345	1270.	-.638E-05	.969E-05	-.100E-05	-.146E-04	-.589E-06	-.268E-05	.499E-05	.794E-05	-.133E-04	-.237E-05	.519E-06	.761E-06
65	.370	1333.	-.124E-04	.137E-04	-.842E-06	-.187E-04	.790E-05	-.368E-05	.105E-04	.185E-04	-.257E-04	-.333E-05	.854E-06	.215E-05
70	.395	1391.	-.187E-04	.165E-04	-.962E-06	-.228E-04	.152E-04	-.445E-05	.158E-04	.284E-04	-.359E-04	-.414E-05	.918E-06	.399E-05
75	.420	1442.	-.241E-04	.166E-04	-.947E-06	-.243E-04	.202E-04	-.482E-05	.208E-04	.353E-04	-.419E-04	-.463E-05	.789E-06	.514E-05
80	.445	1488.	-.280E-04	.157E-04	-.103E-06	-.216E-04	.249E-04	-.465E-05	.219E-04	.387E-04	-.436E-04	-.480E-05	.631E-06	.449E-05
85	.470	1526.	-.304E-04	.160E-04	.210E-05	-.148E-04	.317E-04	-.393E-05	.152E-04	.392E-04	-.416E-04	-.470E-05	.422E-06	.283E-05
90	.495	1559.	-.315E-04	.176E-04	.560E-05	-.604E-05	.407E-04	-.270E-05	.999E-06	.374E-04	-.372E-04	-.431E-05	.150E-06	.126E-05
95	.520	1586.	-.312E-04	.199E-04	.960E-05	.216E-05	.493E-04	-.107E-05	-.159E-04	.328E-04	-.320E-04	-.345E-05	-.193E-06	-.440E-06
100	.545	1608.	-.294E-04	.215E-04	.129E-04	.788E-05	.542E-04	.795E-06	-.293E-04	.246E-04	-.274E-04	-.191E-05	-.609E-06	-.211E-05
105	.570	1627.	-.261E-04	.211E-04	.146E-04	.109E-04	.532E-04	.273E-05	-.355E-04	.129E-04	-.244E-04	.347E-06	-.908E-06	-.281E-05
110	.595	1642.	-.216E-04	.185E-04	.142E-04	.126E-04	.470E-04	.454E-05	-.338E-04	-.579E-06	-.230E-04	.308E-05	-.904E-06	-.264E-05
115	.620	1654.	-.167E-04	.138E-04	.120E-04	.144E-04	.385E-04	.600E-05	-.261E-04	-.125E-04	-.230E-04	.576E-05	-.713E-06	-.238E-05
120	.645	1662.	-.119E-04	.790E-05	.906E-05	.165E-04	.311E-04	.689E-05	-.163E-04	-.201E-04	-.234E-04	.774E-05	-.574E-06	-.196E-05
125	.670	1667.	-.779E-05	.180E-05	.646E-05	.175E-04	.265E-04	.708E-05	-.799E-05	-.226E-04	-.236E-04	.852E-05	-.520E-06	-.115E-05
130	.695	1671.	-.465E-05	-.351E-05	.513E-05	.154E-04	.236E-04	.659E-05	-.197E-05	-.217E-04	-.230E-04	.803E-05	-.424E-06	-.470E-06
135	.720	1674.	-.250E-05	-.734E-05	.546E-05	.993E-05	.199E-04	.560E-05	.249E-05	-.195E-04	-.213E-04	.661E-05	-.249E-06	-.263E-06
140	.745	1677.	-.125E-05	-.937E-05	.716E-05	.321E-05	.138E-04	.436E-05	.550E-05	-.178E-04	-.182E-04	.486E-05	-.933E-07	-.292E-06
145	.770	1679.	-.769E-06	-.982E-05	.949E-05	-.748E-06	.635E-05	.314E-05	.588E-05	-.167E-04	-.132E-04	.335E-05	-.281E-07	-.268E-06
150	.795	1681.	-.862E-06	-.935E-05	.116E-04	.102E-05	.402E-06	.210E-05	.243E-05	-.154E-04	-.689E-05	.235E-05	-.201E-07	-.146E-06
155	.820	1681.	-.130E-05	-.878E-05	.126E-04	.807E-05	-.165E-05	.129E-05	-.384E-05	-.132E-04	-.579E-06	.181E-05	-.186E-07	-.292E-07
160	.845	1681.	-.940E-06	-.855E-05	.123E-04	.165E-04	-.410E-07	.737E-06	-.987E-05	-.104E-04	.328E-05	.144E-05	-.209E-07	.852E-08
165	.870	1681.	-.114E-06	-.852E-05	.105E-04	.214E-04	.282E-05	.467E-06	-.110E-04	-.773E-05	.267E-05	.100E-05	-.196E-07	.138E-09
170	.895	1680.	0.	-.812E-05	.773E-05	.202E-04	.470E-05	.500E-06	-.508E-05	-.592E-05	-.238E-05	.462E-06	-.542E-08	-.533E-08
175	.920	1679.	0.	-.692E-05	.462E-05	.140E-04	.540E-05	.796E-06	.371E-05	-.511E-05	-.913E-05	-.148E-07	0.	-.218E-08
180	.945	1678.	0.	-.507E-05	.220E-05	.651E-05	.631E-05	.120E-05	.898E-05	-.483E-05	-.134E-04	-.204E-06	0.	-.436E-08

TABLE B-2. - Net reaction rate profiles for the species unrelated to the inhibitor in flame IV

			NET REACTION RATE											
INDEX	Z	TEMP	CH4	CO	CO2	H	H2O	OH	A	H2	O2	O	H2CO	CH3
5	.070	300.	.943E-05	.100E-05	.815E-06	.389E-07	.132E-05	0.	-.244E-04	.295E-05	.221E-04	0.	-.117E-07	.143E-07
10	.095	300.	.235E-04	.909E-06	.331E-06	.459E-07	.620E-06	0.	-.167E-04	.124E-04	.259E-04	0.	-.202E-08	.148E-07
15	.120	349.	.237E-04	-.969E-07	-.414E-06	.127E-07	-.172E-05	0.	-.916E-05	.882E-05	.220E-04	0.	-.390E-08	.932E-08
20	.145	427.	.109E-04	-.724E-06	-.813E-06	-.110E-06	-.181E-05	-.360E-08	-.449E-05	-.266E-08	.113E-04	0.	-.109E-08	.608E-08
25	.170	510.	.617E-05	-.683E-06	-.109E-05	-.362E-06	-.179E-05	-.927E-07	-.890E-06	-.250E-05	.681E-05	0.	.517E-08	.523E-08
30	.195	597.	.423E-05	-.853E-06	-.135E-05	-.654E-06	-.330E-05	-.225E-06	.170E-05	-.399E-05	.394E-05	0.	.653E-08	.430E-08
35	.220	684.	.405E-05	-.226E-05	-.178E-05	-.973E-06	-.719E-05	-.267E-06	.510E-05	-.463E-05	.259E-05	0.	.653E-08	.666E-08
40	.245	769.	.476E-05	-.291E-05	-.256E-05	-.116E-05	-.130E-04	-.260E-06	.883E-05	-.467E-05	.205E-05	0.	.805E-08	.136E-07
45	.270	853.	.498E-05	-.409E-05	-.359E-05	-.117E-05	-.185E-04	-.160E-06	.141E-04	-.456E-05	.161E-05	0.	.100E-07	.846E-08
50	.295	934.	.343E-05	-.549E-05	-.454E-05	-.114E-05	-.203E-04	.954E-08	.188E-04	-.410E-05	.139E-05	0.	.974E-08	-.513E-07
55	.320	1014.	.114E-05	-.521E-05	-.488E-05	-.129E-05	-.167E-04	.193E-06	.185E-04	-.399E-05	.108E-05	0.	.788E-08	-.327E-06
60	.345	1090.	-.290E-06	-.339E-05	-.432E-05	-.177E-05	-.854E-05	.321E-06	.119E-04	-.486E-05	.127E-05	0.	.245E-08	-.996E-06
65	.370	1165.	-.104E-06	-.139E-05	-.300E-05	-.255E-05	.393E-06	.354E-06	.182E-05	-.705E-05	.248E-05	0.	-.242E-07	-.157E-05
70	.395	1238.	.179E-05	-.718E-06	-.152E-05	-.328E-05	.573E-05	.284E-06	-.699E-05	-.999E-05	.457E-05	0.	-.724E-07	-.123E-05
75	.420	1307.	.447E-05	-.157E-05	-.608E-06	-.360E-05	.396E-05	.997E-07	-.984E-05	-.122E-04	.702E-05	-.426E-06	-.675E-07	-.729E-06
80	.445	1374.	.618E-05	-.305E-05	-.824E-06	-.368E-05	-.443E-05	-.274E-06	-.457E-05	-.115E-04	.899E-05	-.145E-05	-.475E-08	-.175E-05
85	.470	1436.	.560E-05	-.433E-05	-.228E-05	-.473E-05	-.158E-04	-.982E-06	.625E-05	-.611E-05	.994E-05	-.194E-05	.217E-07	-.349E-05
90	.495	1495.	.253E-05	-.249E-05	-.444E-05	-.891E-05	-.251E-04	-.217E-05	.153E-04	.474E-05	.926E-05	-.188E-05	-.508E-07	-.338E-05
95	.520	1549.	-.247E-05	.435E-05	-.624E-05	-.181E-04	-.271E-04	-.389E-05	.166E-04	.199E-04	.602E-05	-.147E-05	-.131E-06	-.105E-05
100	.545	1598.	-.864E-05	.138E-04	-.647E-05	-.318E-04	-.194E-04	-.603E-05	.108E-04	.365E-04	-.996E-06	-.136E-05	-.594E-07	.253E-05
105	.570	1643.	-.157E-04	.226E-04	-.446E-05	-.464E-04	-.275E-05	-.831E-05	.296E-05	.509E-04	-.121E-04	-.250E-05	.114E-07	.721E-05
110	.595	1684.	-.238E-04	.298E-04	-.736E-06	-.555E-04	.180E-04	-.104E-04	-.272E-05	.596E-04	-.263E-04	-.535E-05	.173E-06	.116E-04
115	.620	1720.	-.326E-04	.348E-04	.314E-05	-.533E-04	.368E-04	-.116E-04	-.254E-05	.605E-04	-.413E-04	-.924E-05	.746E-06	.124E-04
120	.645	1751.	-.408E-04	.372E-04	.556E-05	-.382E-04	.489E-04	-.115E-04	.574E-05	.537E-04	-.539E-04	-.124E-04	.896E-06	.789E-05
125	.670	1779.	-.458E-04	.366E-04	.621E-05	-.143E-04	.539E-04	-.911E-05	.164E-04	.408E-04	-.613E-04	-.126E-04	.269E-06	.646E-06
130	.695	1802.	-.456E-04	.330E-04	.651E-05	.100E-04	.550E-04	-.425E-05	.172E-04	.249E-04	-.617E-04	-.897E-05	-.935E-07	-.470E-05
135	.720	1821.	-.398E-04	.266E-04	.860E-05	.268E-04	.569E-04	.262E-05	.236E-05	.853E-05	-.554E-04	-.214E-05	-.190E-07	-.635E-05
140	.745	1835.	-.303E-04	.185E-04	.135E-04	.329E-04	.617E-04	.100E-04	-.232E-04	-.609E-05	-.451E-04	.558E-05	.361E-07	-.579E-05
145	.770	1847.	-.200E-04	.102E-04	.201E-04	.309E-04	.676E-04	.158E-04	-.487E-04	-.179E-04	-.347E-04	.116E-04	-.207E-06	-.436E-05
150	.795	1855.	-.115E-04	.284E-05	.252E-04	.264E-04	.698E-04	.184E-04	-.629E-04	-.262E-04	-.273E-04	.143E-04	-.520E-06	-.250E-05
155	.820	1860.	-.593E-05	-.319E-05	.258E-04	.242E-04	.632E-04	.173E-04	-.591E-04	-.306E-04	-.235E-04	.138E-04	-.595E-06	-.103E-05
160	.845	1863.	-.313E-05	-.798E-05	.214E-04	.252E-04	.468E-04	.133E-04	-.389E-04	-.308E-04	-.215E-04	.112E-04	-.257E-06	-.547E-06
165	.870	1865.	-.206E-05	-.117E-04	.138E-04	.266E-04	.244E-04	.826E-05	-.111E-04	-.275E-04	-.189E-04	.804E-05	-.152E-07	-.877E-06
170	.895	1866.	-.172E-05	-.140E-04	.684E-05	.254E-04	.350E-05	.388E-05	.124E-04	-.223E-04	-.150E-04	.536E-05	0.	-.905E-06
175	.920	1866.	-.138E-05	-.144E-04	.343E-05	.205E-04	-.953E-05	.102E-05	.237E-04	-.172E-04	-.111E-04	.344E-05	0.	-.248E-06
180	.945	1866.	-.452E-06	-.124E-04	.411E-05	.133E-04	-.126E-04	-.315E-06	.230E-04	-.137E-04	-.906E-05	.216E-05	0.	0.

TABLE B-3. - Net reaction rate profiles for the species related to the inhibitor in flame IV

NET REACTION RATE

INDEX	Z	TEMP	CF3BR	HF	HBR	BR	CH3BR	HCO	F2CO	CH2CF2	HO2	BR2	CF3H	CF2
5	.070	300.	-.372E-06	.598E-06	.219E-07	0.	-.136E-08	0.	.181E-07	.207E-07	0.	.435E-08	.148E-08	-.192E-07
10	.095	300.	-.215E-05	.568E-06	.898E-08	0.	-.473E-09	0.	-.281E-09	-.196E-07	0.	.229E-08	.812E-09	.100E-08
15	.120	349.	-.237E-05	-.768E-07	-.390E-07	0.	-.103E-08	0.	-.279E-07	-.472E-07	0.	-.477E-09	-.975E-09	.328E-08
20	.145	427.	-.108E-05	-.427E-06	-.902E-07	-.552E-07	-.103E-08	0.	-.415E-07	-.420E-07	0.	-.998E-10	-.376E-10	.382E-08
25	.170	510.	-.593E-06	-.543E-06	-.132E-06	-.374E-06	-.765E-08	0.	-.498E-07	-.114E-07	0.	.156E-08	.350E-08	-.597E-08
30	.195	597.	-.286E-06	-.645E-06	-.107E-06	-.697E-06	-.186E-07	0.	-.499E-07	-.143E-07	0.	.417E-08	.421E-08	-.235E-07
35	.220	684.	.177E-07	-.781E-06	-.201E-07	-.913E-06	-.264E-07	0.	-.422E-07	-.632E-07	0.	.814E-08	-.472E-08	-.429E-07
40	.245	769.	.361E-06	-.101E-05	.473E-07	-.109E-05	-.250E-07	0.	-.298E-07	-.103E-06	0.	.154E-07	-.139E-07	-.604E-07
45	.270	853.	.878E-06	-.127E-05	.802E-08	-.119E-05	-.146E-07	0.	-.136E-07	-.120E-06	0.	.230E-07	-.111E-07	-.750E-07
50	.295	934.	.146E-05	-.142E-05	-.141E-06	-.124E-05	.120E-08	0.	.494E-08	-.114E-06	0.	.210E-07	-.379E-09	-.871E-07
55	.320	1014.	.191E-05	-.132E-05	-.223E-06	-.126E-05	.226E-07	0.	.236E-07	-.266E-07	0.	.651E-08	.526E-08	-.952E-07
60	.345	1090.	.213E-05	-.900E-06	-.313E-07	-.122E-05	.558E-07	0.	.400E-07	.122E-06	0.	-.909E-08	-.407E-08	-.917E-07
65	.370	1165.	.207E-05	-.316E-05	.321E-06	-.105E-05	.103E-06	0.	.498E-07	.158E-06	0.	-.152E-07	-.130E-07	-.616E-07
70	.395	1238.	.175E-05	.140E-06	.490E-06	-.703E-06	.151E-06	0.	.498E-07	.157E-07	0.	-.114E-07	.200E-08	.135E-07
75	.420	1307.	.120E-05	.417E-06	.412E-06	-.145E-06	.192E-06	0.	.443E-07	-.153E-07	0.	-.910E-08	.245E-07	.147E-06
80	.445	1374.	.491E-06	.490E-06	.369E-06	.580E-06	.224E-06	0.	.494E-07	.342E-06	0.	-.103E-07	.212E-07	.333E-06
85	.470	1436.	-.432E-06	.739E-06	.584E-06	.139E-05	.247E-06	0.	.882E-07	.820E-06	0.	-.111E-07	.142E-07	.541E-06
90	.495	1495.	-.164E-05	.153E-05	.980E-06	.218E-05	.239E-06	0.	.181E-06	.107E-05	0.	-.112E-07	.393E-07	.708E-06
95	.520	1549.	-.307E-05	.303E-05	.130E-05	.282E-05	.156E-06	0.	.330E-06	.136E-05	0.	-.759E-08	.683E-07	.767E-06
100	.545	1598.	-.447E-05	.506E-05	.145E-05	.319E-05	-.176E-07	0.	.510E-06	.168E-05	0.	-.285E-08	.680E-07	.669E-06
105	.570	1643.	-.545E-05	.724E-05	.151E-05	.326E-05	-.206E-06	0.	.676E-06	.121E-05	0.	-.115E-08	.545E-07	.416E-06
110	.595	1684.	-.569E-05	.911E-05	.145E-05	.313E-05	-.298E-06	0.	.782E-06	-.196E-07	0.	-.185E-08	.437E-07	.682E-07
115	.620	1720.	-.512E-05	.102E-04	.984E-06	.302E-05	-.258E-06	0.	.808E-06	-.931E-06	0.	-.214E-08	.297E-07	-.277E-06
120	.645	1751.	-.399E-05	.103E-04	-.358E-07	.314E-05	-.160E-06	0.	.765E-06	-.118E-05	0.	-.169E-08	.806E-08	-.526E-06
125	.670	1779.	-.269E-05	.933E-05	-.120E-05	.348E-05	-.104E-06	0.	.684E-06	-.114E-05	0.	-.143E-08	-.171E-07	-.624E-06
130	.695	1802.	-.158E-05	.737E-05	-.182E-05	.380E-05	-.908E-07	0.	.583E-06	-.916E-06	0.	-.159E-08	-.347E-07	-.575E-06
135	.720	1821.	-.826E-06	.493E-05	-.171E-05	.377E-05	-.610E-07	0.	.463E-06	-.657E-06	0.	-.233E-08	-.404E-07	-.434E-06
140	.745	1835.	-.363E-06	.258E-05	-.124E-05	.322E-05	-.825E-08	0.	.318E-06	-.554E-06	0.	-.283E-08	-.417E-07	-.269E-06
145	.770	1847.	-.825E-07	.782E-06	-.796E-06	.229E-05	.172E-07	0.	.154E-06	-.451E-06	0.	-.130E-08	-.375E-07	-.137E-06
150	.795	1855.	-.199E-08	-.257E-06	-.529E-06	.128E-05	-.320E-08	0.	-.459E-08	-.208E-06	0.	-.890E-10	-.230E-07	-.573E-07
155	.820	1860.	0.	-.597E-06	-.379E-06	.506E-06	-.341E-07	0.	-.126E-06	-.309E-07	0.	0.	-.965E-08	-.238E-07
160	.845	1863.	0.	-.430E-06	-.268E-06	.960E-07	-.222E-07	0.	-.194E-06	0.	0.	0.	-.126E-07	-.152E-07
165	.870	1865.	0.	.233E-07	-.177E-06	-.141E-07	-.192E-08	0.	-.216E-06	0.	0.	0.	-.258E-07	-.131E-07
170	.895	1866.	0.	.536E-06	-.115E-06	.193E-07	0.	0.	-.211E-06	0.	0.	0.	-.300E-07	-.935E-08
175	.920	1866.	0.	.885E-06	-.687E-07	.632E-07	0.	0.	-.196E-06	0.	0.	0.	-.212E-07	-.273E-08
180	.945	1866.	0.	.909E-06	-.212E-07	.631E-07	0.	0.	-.174E-06	0.	0.	0.	-.140E-07	0.

APPENDIX C.--LIST OF SYMBOLS

Symbol	Units	Definition
A	-	Area expansion ratio.
amu	-	Atomic mass units.
D_{i-Ar}	$cm^2\ sec^{-1}$	Binary diffusion coefficient of species i with argon.
G_i	-	Fractional mass flux of species i.
I_m	-	Mass spectral intensity at mass m.
K	-	Degrees kelvin.
K_i	moles $cm^{-3}\ sec^{-1}$	Net reaction rate of species i.
k_j	sec^{-1} (1st order) $cm^3\ mole^{-1}\ sec^{-1}$ (2d order) $cm^6\ mole^{-2}\ sec^{-1}$ (3d order)	Chemical reaction rate coefficient of reaction j.
k_{T_i}	-	Thermal diffusion ratio of species i.
M_i	$g\ mole^{-1}$	Gram molecular weight of species i.
RRK	-	Rice-Ramsperger-Kassel theory of unimolecular reactions.
T	K	Temperature.
v	$cm\ sec^{-1}$	Bulk flow velocity.
X_i	-	Mole fraction of species i.
z	cm	Perpendicular distance from the burner surface to sampling probe tip.
ρ	$g\ cm^{-3}$	Mean mass density.

☆U.S. GOVERNMENT PRINTING OFFICE: 1978-703-103/70

INT.-BU.OF MINES,PGH.,PA. 23235